Article

Price and carbon-based energy flexibility of residential heating and cooling loads using model predictive control

Academic Editor: name
Received: date; Accepted: date; Published: date

Declarations of interest: None.

Abstract: Model predictive controllers (MPC) have shown great potential for activating the energy flexibility of thermal loads, especially in buildings equipped with heat pump systems. In this work, an MPC controller is developed and tested within a co-simulation framework which couples an optimization software with a dynamic building simulation tool. The development phase is described in detail, in particular the methods to obtain simplified models to be used by the controller. The building envelope and the heat pump performance (based on experimental data) were thus modelled, both in heating and cooling seasons. Three different objective functions of the MPC are tested on a study case consisting of a Spanish residential building: promising results are obtained when the controller aims at minimizing operational costs (savings of 13 to 29%) or CO_2 marginal emissions (savings of 19 to 29%). The development efforts, the required tuning and sensitivity of the MPC algorithm parameters, the adaptations needed between the cooling and heating operations are also discussed and put into perspective with the obtained benefits in terms of savings, comfort and load-shifting.

Keywords: model predictive control; energy flexibility; carbon footprint minimization; variable speed heat pump; heating and cooling loads; co-simulation; HVAC control; heat pump control.

1. Introduction

The latest report of the Intergovernmental Panel on Climate Change (IPCC) establishes clearly that the Earth has already warmed on average by 1°C compared to pre-industrial levels, and that global warming will certainly reach at least 1.5°C by 2030 due to manmade activities [1]. To avoid going beyond 1.5°C and the catastrophic consequences related to such an important climate change, the IPCC calls among other recommendations for a deep and fast decarbonization of our energy systems. The introduction of a large share of renewable sources of energy has therefore become an absolute and urgent necessity. However, this transition might provoke challenges and instability in the electricity grids, if non-dispatchable sources such as solar and wind become predominant. Some regions already experience the effects of a high penetration of renewable energy sources (RES): in California or Germany for example, where the share of solar energy is high, prices can become negative at times of high production. In such cases, curtailment of the RES constitutes an easy solution, but basically consist in wasting free available energy, like these days of December 2012 where 300 MW of wind power were curtailed in Germany [2].

This situation calls for better solutions, and notably for an increase in the flexibility of the demand side. The momentum towards a more flexible electricity system based on RES is increasing [3] and it has definitely become a "hot topic", given the large amount of literature recently published on the matter [2]. Through an increased flexibility, energy systems could have inherent capabilities

to accommodate a larger share of variable RES without requiring massive new investments. In particular, treating thermal and electrical systems as a whole could offer major new opportunities [2]. Along this line, enhancing the flexibility of buildings energy use has concentrated an important amount of research [4]. Buildings possess an inherent thermal mass which can be regarded as a storage means and activated by appropriate control strategies [5]. Additional storage options such as water tanks or embedded phase-change materials can also be valued for that purpose [6]. Heating, Ventilation and Air Conditioning (HVAC) systems operate inherently shiftable loads which can contribute to the energy flexibility of a building, and heat pumps in particular show a promising potential as a means to couple the electrical grids with thermal storages and to provide demand-side management [7].

To unlock the flexibility potential of heat pumps in buildings, smart controls are required, which can take the form of simple rule-based controls or model predictive controls (MPC) [8]. In the present work, the focus lies on indirect control, i.e. strategies that provide an incentive signal such as a variable electricity price, and then let the end users (or a controller for them) decide whether to react or not. MPC has been extensively studied in recent years for such control strategies in building climate control [9]–[11]. However, it has still not been widely applied in the control of real buildings, and many aspects require further investigations. For these reasons, the authors are presenting in this study the development and testing of an MPC controller for enhancing the energy flexibility of residential buildings equipped with heat pumps in Spain. Identifying the current lacks in this field of investigation, the motivations behind this research can be summarized with the following points:

- The formulation of the Optimal Control Problem (OCP) in MPC has already been discussed in previous literature [12], in particular the linear modelling of variable speed heat pump (VSHP) performance. However, such formulations only resorted to linear programming (without integer variables), and thus could not reproduce the switching of the heat pump between different modes (like space heating/cooling on one hand and production of Domestic Hot Water (DHW) on the other hand), nor the switching off of the heat pump below certain load level. In the present work, the authors propose a different OCP including integer variables, which increases the complexity of the MPC, but enables to reproduce a more realistic behavior of the systems. It also corresponds to the commands that can be sent to control a real heat pump, which brings this research one step closer to an implementation with real systems. Furthermore, the modelling of the heat pump performance is here realized with experimental data instead of more commonly used manufacturer's data, which are often incomplete and display the performance of the heat pump in ideal conditions.
- In a previous literature review [8], it was noted that the great majority of published research on the present topic used economic optimization, which means these controllers receive a variable price signal and intend to minimize the corresponding energy costs. It was suggested that other objective functions could be studied, since the ultimate goal is actually to reduce the carbon footprint of our energy use. In this regard, the grid carbon intensity has been used in recent research as an alternative input signal for MPC in HVAC control [13], [14]. In the present work, the authors propose to use a model of the *marginal* CO_2 emissions [15], instead of the average emissions of the electrical grid. The marginal emissions consider the merit order in which the production plants are activated in a given grid, and thus the emissions savings are meant to be calculated more accurately. For instance, if a demand-side management action triggers a reduction of the energy use, this will not affect a base plant like nuclear, which is too slow to start and stop for balancing the grid. Instead, this variation will be compensated for example by a gas turbine, and therefore the resulting marginal emissions saved will be greater. The Marginal Emissions Factor (MEF) will thus be used in this study, as it represents a novel and more appropriate input signal for reducing the CO_2 emissions in an MPC framework.
- MPC has shown great potential in prior research for managing HVAC systems in buildings, and increase their demand-side flexibility. However, the development costs of such

technology remain high [16]: it was found for example that the creation of suitable control models account for 50 to 80% of the development costs [17]. Furthermore, the computation efforts also remain high in certain MPC configurations. These obstacles notably explain the still low market penetration of MPC controllers despite their repeatedly proven performance in building climate control. The development efforts of the MPC will therefore be explained and analyzed in details in this study.

- To the knowledge of the authors, an MPC framework enhancing the flexibility of both heating and cooling loads in different seasons has seldom been studied. The present article will relate the adaptations needed to apply MPC in the same building in summer and winter, with the same reversible heat pump that can provide space heating or cooling. In particular, the adaptations needed in the models (building envelope, heat pump performance) and the MPC formulation will be discussed.
- Finally, a co-simulation platform for testing MPC configurations will be presented. In this case, TRNSYS is used as a dynamic simulation software to emulate the behavior of a virtual building in details. MATLAB is used as the optimization software in which the MPC controller is implemented. Coupling these two powerful tools enables to benefit from the very accurate simulation results of TRNSYS, while overcoming its limitations, since it cannot integrate predictive controllers directly [18]. The overall co-simulation framework will here be used to test different MPC configurations, and could be reused as a benchmark for later studies, notably to perform sensitivity analysis on the multiple parameters of the MPC controller, or with different building typologies, for example including on-site RES production.

The article is structured as follows: firstly, the methods section introduce the development and implementation process of the MPC controller. The overall co-simulation framework is laid out to set the context of the work. The study case and the building model identification process are then described: this work focuses on residential building in the Mediterranean area, therefore this typology is modelled. The performance of a VSHP is also modelled based on experimental data obtained in a laboratory setup. The whole MPC algorithm is then detailed, focusing on the different objective functions tested: minimization of delivered thermal energy, of the electricity costs or the CO_2 marginal emissions due to the heat pump operation. Simulations of three days duration were carried out in this framework, with different MPC configurations, both in heating and cooling mode: they are reported in the results section. The analysis focuses on the following aspects: energy flexibility, levels of thermal and electrical energy, efficiency of the systems, monetary costs, CO_2 marginal emissions and comfort of the occupants. Finally, the benefits and drawbacks of MPC are discussed, in particular the development efforts required by such technology, its high sensitivity to certain parameters and the confirmed benefits it can provide. Conclusions are drawn in the final chapter.

2. Methods: implementation of a Model Predictive Control framework

2.1. Co-simulation framework with MATLAB and TRNSYS

To test different configurations, a co-simulation framework has been implemented. In this scheme, the detailed model in TRNSYS serves as the "real building", in other words it constitutes a virtual plant with which the control strategies can be tested. TRNSYS does not contain suitable tools for optimization, therefore the MPC calculation must be externalized in another software, MATLAB in the present case. For clarity, the term "detailed" generally refers to the TRNSYS framework, while the term "simplified" refers to the MPC framework (the models and time steps of these two frameworks are notably distinct). The scheme of the co-simulation and the exchange of variables is presented in Figure 1. The TRNSYS simulation runs using the necessary inputs (weather, occupancy grid etc…) from external files. When the MPC controller in MATLAB is called, it is provided with the

necessary input (the initial values of the states and the forecasts for the next 24h taken from the same files).

In MATLAB, the control problem is formulated with the YALMIP tool [19] and solved with GUROBI [20]. To limit the computation efforts, the MPC controller requires simplified or low order models of the building envelope and the heat pump performance: these are detailed respectively in sections 2.2 and 2.3. From the optimal control trajectory calculated over the horizon of the next 24 hours, only the first values are sent to TRNSYS, before a new computation of the MPC is carried out and new values are obtained. In practice, the Type155 of TRNSYS enables to establish the connection between both software.

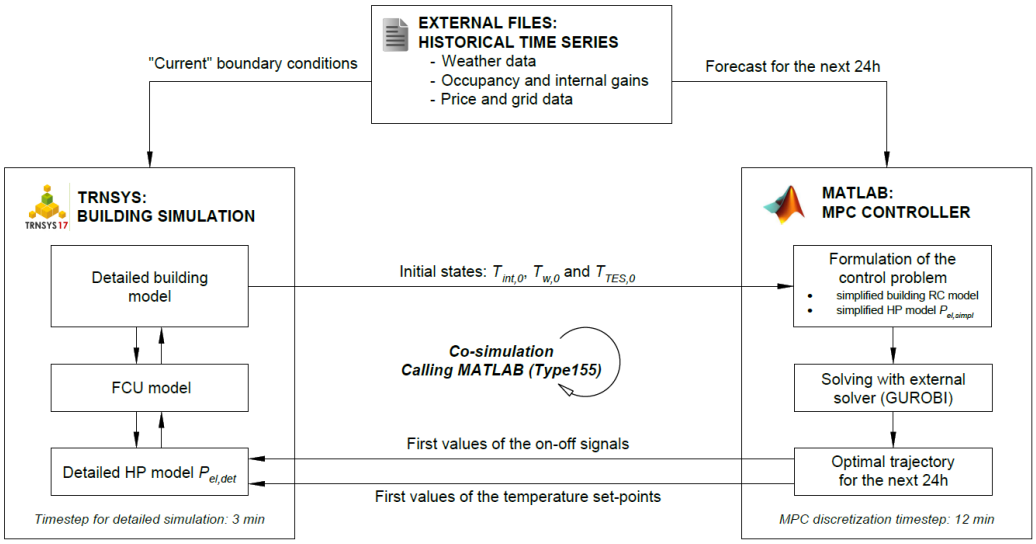

Figure 1. Co-simulation scheme between TRNSYS and MATLAB.

2.2. Building modelling

2.2.1. Study case and detailed model

The present study focuses on the Mediterranean climate and the typical residential buildings constructed in this zone. They present the characteristics of having relatively balanced heating and cooling loads in winter and summer. Therefore such buildings can be used for demand response in both seasons. However, despite the great amount of literature on MPC and building energy flexibility published in the recent years, few studies have focused on cooling applications, and even less on study cases that make use of flexibility in both seasons [8]. Given this state of the art, the authors have deemed worthy to investigate in more details the potential of energy flexibility of Mediterranean buildings.

A typical block of flats of the region of Catalonia in Spain was chosen as a case study. In particular, one flat situated on the first floor is studied in details. The apartment, where lives a family of four, comprises 4 bedrooms, a living room, kitchen and bathroom for a total surface of 110 m^2. The external walls contain 12 cm of insulation which represents a high insulation level for the Spanish climate. The HVAC systems comprise an air-to-water heat pump which provides heating or cooling to the Fan-Coil Units (FCU) situated in the rooms. The heat pump also contains an integrated 200 liters tank for storing DHW. The apartment is simulated in TRNSYS, with a detailed model that was previously validated with experimental metered data [21], [22]. This detailed model runs with a time step of 3 minutes, enabling to capture short-term variations with sufficient accuracy.

2.2.2. Reduced order simplified RC model: structure and variables

For reasons of computation effort, simplified and linear models are necessary in the MPC framework to predict the dynamic behavior of the building [23]. A state-space model of the building study case was thus developed and identified through grey-box modelling techniques. The structure

represented in Figure 2 was chosen, with three temperature states $\boldsymbol{x} = [T_{int}\ T_w\ T_{TES}]^T$: the indoor temperature, an intermediate temperature at the inside surface of the walls, and the average water tank temperature. It should be emphasized that such simplified models are developed only for control purposes, and not for matching exactly with the real building structure, therefore the level of details is kept to a minimum.

The first state T_{int} lumps all the rooms of the apartment into one single operative temperature state, which is sufficient for MPC applications as shown for example in [24]. Its associated capacity C_{int} mostly represents the heat capacity of the air, furniture and internal partitions present within the entire inside zone, and considered as a single body [25], [26]. Lumping these elements of different thermal capacities into the single parameter C_{int} represents an important simplification, however the purpose of the simplified model is only to provide a general prediction of the building dynamics for the controller, and in this scope such assumption is valid, even if the physical phenomena are not represented in the most accurate manner. External heat inputs enter the building at the level of the state T_{int}: the heat naturally emitted by the occupants and the equipment Q_{occ}, the heat gains due to the ground horizontal solar irradiation I_H (buffered by the aperture area coefficient gA) and the heat Q_S provided by the FCU and heat pump system (negative in case of cooling).

The second state T_w represents an intermediate temperature at the surface of the external walls, and its associated capacity C_w covers the heat capacity of the massive walls. T_w is linked with the outside temperature T_{amb} through the resistance of the walls R_w. The different dynamics of the two states are therefore both captured by this type of model. A first order model lumping all the thermal capacitance into a single parameter would not have been able to capture both the fast dynamics of the indoor zone and the slower dynamics of the massive structural elements. On the other hand, a third order model with an additional capacity accounting for internal walls and/or furniture could represent an alternative modelling approach, but adding unknown parameters increases the complexity of the obtained model and of the identification process. The second order modelling approach presented here is thus considered sufficient for MPC applications [26], and was used in many previous works as shown in the introductory review of [27].

Moreover, the DHW tank constitutes an additional state T_{TES}, which represents the average water temperature of the tank under a fully mixed tank assumption. The capacity C_{TES} covers the heat capacity of the 200 liters of water and the resistance R_{TES} takes into account the insulation of the tank. The DHW tank is charged through the heat Q_{TES} (positive term) coming from the heat pump circuit, and discharged with the heat tapped by the occupants Q_{DHW} (negative term, which follows the deterministic tapping program L from the standard [28]).

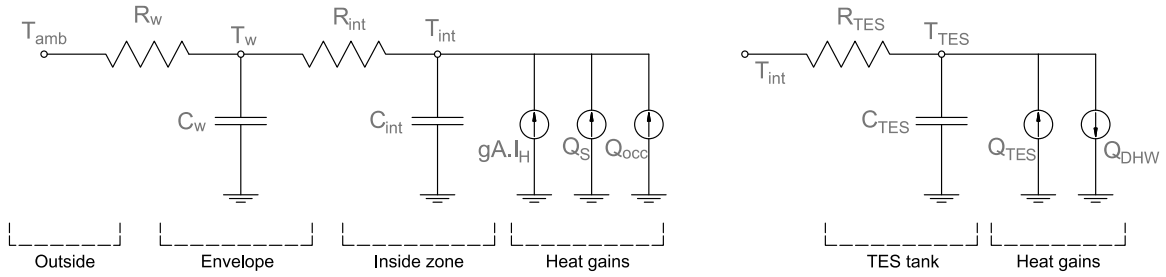

Figure 2. Representation of the simplified RC model.

To conform to the state-space model format, the model takes the form of Eq.(1), which stems from writing the differential equations ruling the heat transfers of every state. For clarity, the matrix $\boldsymbol{B}$ is separated into $\boldsymbol{B_u}$, which corresponds to the controllable inputs $\boldsymbol{u} = [Q_S\ Q_{TES}]^T$, and $\boldsymbol{B_e}$ which corresponds to the exogenous, non-controllable inputs $\boldsymbol{e} = [T_{amb}\ I_H\ Q_{occ}\ Q_{DHW}]^T$. The considered relevant outputs are $\boldsymbol{y} = [T_{int}\ T_{TES}]^T$. The continuous time model is discretized using a 12 minutes sampling time for use into the discrete MPC scheme.

$$\begin{cases} \dot{\boldsymbol{x}} = \boldsymbol{A} \cdot \boldsymbol{x} + \boldsymbol{B_u} \cdot \boldsymbol{u} + \boldsymbol{B_e} \cdot \boldsymbol{e} \\ \boldsymbol{y} = \boldsymbol{C} \cdot \boldsymbol{x} \end{cases} \quad (1)$$

With:

$$\boldsymbol{A} = \begin{bmatrix} -\frac{1}{R_{int}C_{int}} & \frac{1}{R_{int}C_{int}} & 0 \\ \frac{1}{R_{int}C_w} & -\frac{1}{R_wC_w} - \frac{1}{R_{int}C_w} & 0 \\ \frac{1}{R_{TES}C_{TES}} & 0 & -\frac{1}{R_{TES}C_{TES}} \end{bmatrix}, \quad \boldsymbol{B_u} = \begin{bmatrix} \frac{1}{C_{int}} & 0 \\ 0 & 0 \\ 0 & \frac{1}{C_{TES}} \end{bmatrix},$$

$$\boldsymbol{B_e} = \begin{bmatrix} 0 & \frac{gA}{C_{int}} & \frac{1}{C_{int}} & 0 \\ \frac{1}{R_wC_w} & 0 & 0 & 0 \\ 0 & 0 & 0 & -\frac{1}{C_{TES}} \end{bmatrix} \text{ and } \boldsymbol{C} = \begin{bmatrix} 1 & 0 & 0 \\ 0 & 0 & 1 \end{bmatrix}$$

2.2.3. Reduced order simplified RC model: identification process

The building part of this RC model was identified with data generated by the detailed model created and previously validated in TRNSYS [21]. The parameters to be identified were R_{int}, C_{int}, R_w, C_w and gA (R_{TES} and C_{TES} were assumed based on manufacturer datasheets). The inputs were the outdoor temperature T_{amb}, the ground horizontal solar irradiation I_H and the total heat provided to the indoor zone $Q_{occ} + Q_S$. In order to have enough dynamic content in the generated data, the building model was excited following a Pseudo Random Binary Signal (PRBS) of the heating Q_S, similarly to the methodology described in [29] and the guidelines of the IEA EBC Annex 68 [30]. The PRBS contains on-off cycles at different frequencies so that both the fast and slow responses of the building are captured in the data, making the identification of the parameters easier and more reliable. Finally, the observation measurements consisted of the temperatures of the states T_{int} and T_w. The model identification was realized with the system identification toolbox of MATLAB [31] ("greyest" method which uses Gauss Newton least square search), and the data generated covered 1400 hours, with time steps of 3 minutes. The results for heating season are presented in Figure 3 and Table 1 (first row). The obtained fit reached 82.3%, which is satisfactory considering the low order of the simplified model.

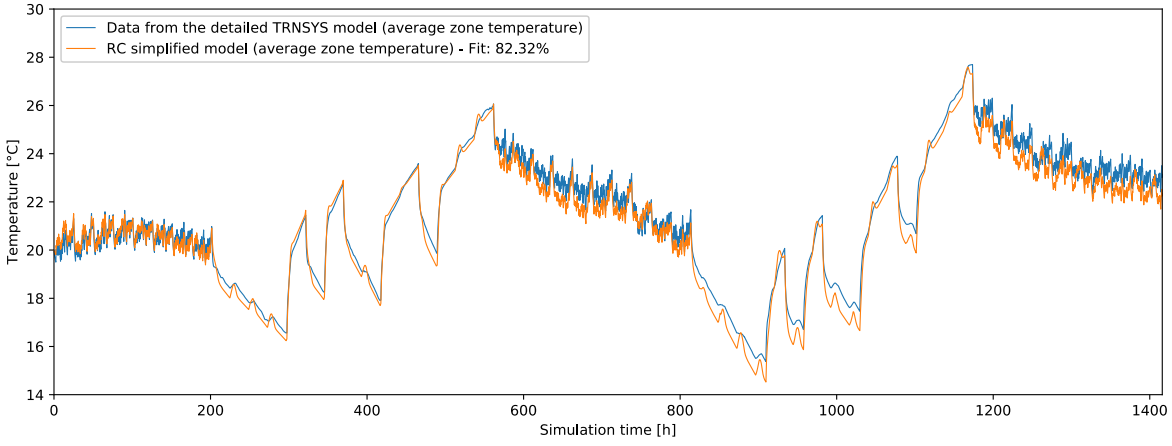

Figure 3. Representation of the data (generated by a detailed model in TRNSYS) and the fitted RC model in heating mode.

The RC model preserves a certain structure which can be interpreted physically, therefore the resistance and capacity values can be compared to an order of magnitude expected for these parameters. Since a lot of smaller parameters are lumped into a limited number of R and C values (4 in this case), it can still result a difficult task to find suitable comparisons. Furthermore, the virtual intermediate state T_w can "move" within the thickness of the wall, which would modify the balance

between the inside zone values (indexed int) and the wall values (indexed w). However, the overall resistance $R_{int} + R_w$ and the overall capacity $C_{int} + C_w$ should remain approximately at the same level. In the present case, the RC model gives $R_{int} + R_w = 10.1\ K/kW$. When considering the resistance of the materials in all individual layers of the external walls, a parallel calculation gives $R_{eq} = 11.5\ K/kW$, which is relatively close. For the capacities, we obtain $C_{int} + C_w = 26.0\ kWh/K$. Summing all the capacities of the materials in the building gives $C_{eq} = 41\ kWh/K$. However, only a part of the external walls mass is activated by the heating of the room (mostly until the insulation layer), the most external layers not being affected by a change of the indoor air temperature [25]. This concept is known as the effective capacity C_{eff}, and is calculated as a portion of C_{eq}. The ratio can vary in a great range and is not known precisely; values ranging from 1/2 to 1/3 are for example mentioned in [32]. Applying this rule to the present case $C_{eff} = 1/3 \cdot C_{eq} = 13.7\ kWh/K$, which should be compared to $26.0\ kWh/K$. A discrepancy is observed, in fact the ratio in the present case is closer to 2/3: $C_{int} + C_w = 0.63 \cdot C_{eq}$. Since there does not exist any agreement in the literature about the calculation of the effective capacity, it is preferred to keep the values originating from the model identification process, given that they offer a good fit with the data, and that the primary goal of the model consists in predicting well rather than being physically meaningful. Furthermore, the balance between the wall and the inside zone values is conserved with the obtained values of R and C: R_w and C_w are much greater than R_{int} and C_{int} respectively, which is expected since the massive walls have a higher resistance and capacity than the air of the inside zone.

Table 1. Parameters of the RC model for heating and cooling.

Coefficient	R_{int}	R_w	R_{TES}	C_{int}	C_w	C_{TES}	gA
Unit	K/kW	K/kW	K/kW	kWh/K	kWh/K	kWh/K	m²
Value (heating)	1.089	9.013	601	1.771	24.22	0.29	1.948
Value (cooling)	0.286	9.404	601	1.771	45.648	0.29	1.558

Theoretically, the values of resistances and capacities obtained in the heating case should also be valid for the cooling case, since they are intrinsic parameters of the building. However, they are subject to changes, for instance the thermal resistance or capacity of a material depend on its temperature, therefore the situation varies with the different boundary conditions in winter and summer. This is especially true for the aperture area gA, which represents the proportion of the outside solar irradiation entering the building, since the sun angle changes significantly between seasons. It can be observed in Figure 4 that keeping the same parameters results in a poor model fit (38.5%) and the apparition of temperature peaks in the cooling season. For this reason, the model identification process is repeated in the cooling mode; this illustrates the limits of using simplified models. The methodology remains the same however: the building is virtually excited with a PRBS signal on the cooling parameter Q_S, which is negative in this case. The parameters obtained for the heating case are used as initial values of this identification process.

The obtained values of the parameters for cooling are presented in the second row of Table 1. The simulation results of this model are compared in Figure 4 with the original TRNSYS model and with the simulation results the heating RC model would have given in the cooling scenario. The total resistance of the model $R_{int} + R_w = 9.69\ K/kW$ stays stable compared to the heating case ($10.1\ K/kW$), although the internal resistance has decreased. On the other hand, the total capacity increases to $C_{int} + C_w = 47.4\ kWh/K$ (compared to $26.0\ kWh/K$ in heating). One possible explanation resides in the fact that in reality, the solar irradiation also hits the wall directly (and thus affects the intermediate state T_w), and this phenomenon has greater amplitude in summer. Since this is not represented in the chosen RC model, the parameter estimation process instead decreased the resistance R_{int} between the two states, so that the external input I_H also affects the state T_w in a more direct manner. As a compensation for this reduced resistance, the capacity state C_w is increased to act as a buffer. Moreover, the aperture area gA has decreased in the cooling model, since the sun angle is higher and thus direct irradiation do not penetrate as deep into the building as in the heating case.

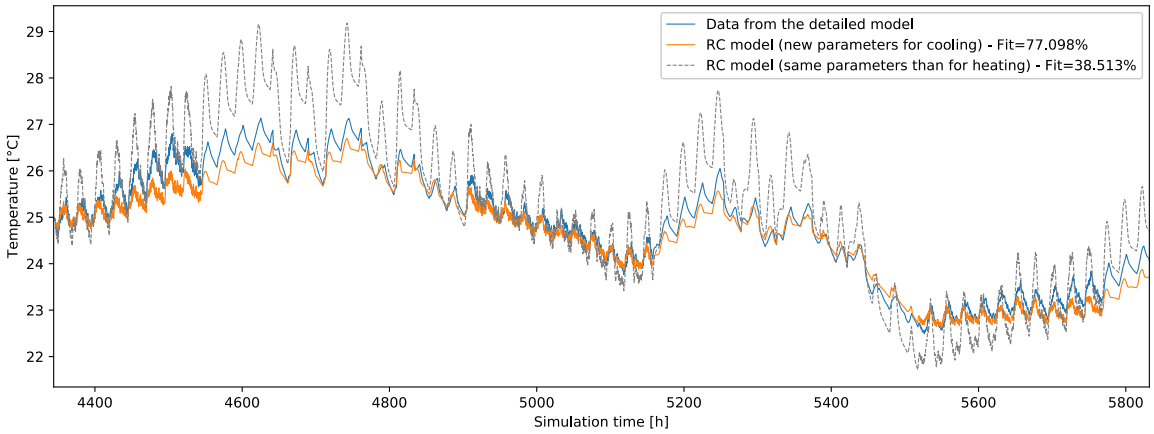

Figure 4. Two different fittings of the RC model for cooling.

The parameter estimation process enabled to emphasize that simplified models for MPC applications in heating and cooling mode should be differentiated. In fact, the RC model simply is a linearization of a detailed model (or a real building) around an operation point; and since this operation point changes significantly between winter and summer, it is preferable to adapt the model as well. In the present case, the RC model was obtained from data created by another, more detailed model, but the identification process would be similar with monitoring data recorded from a real building, although some challenges would arise with the uncertainties of the input data, or if the wall temperature measurement is needed.

2.3. Modelling of heat pump performance from experimental static tests data

When the MPC controller considers the electricity use of the system (see later section 2.5), a model of its performance needs to be provided within its objective function, in order to pass from the thermal energy (determined by the MPC algorithm) to the corresponding consumption of the heat pump. This performance evaluation most often takes the form of a Coefficient of Performance (COP), where $COP = Q/P_{el}$, the ratio between the thermal power Q and electrical power P_{el}. The COP of a VSHP depends on various parameters among which the supply temperature T_{sup}, the ambient temperature T_{amb}, the frequency of the compressor f, the part-load ratio PLR, the absolute value of the thermal power Q, the temperature difference between water supply and return ΔT [12], [33], [34]. Some of these parameters are strongly correlated (e.g. the heat pump will work at lower frequency if the part-load ratio is lower), therefore selecting a subset of these parameters will be sufficient to obtain a reliable model of the heat pump performance.

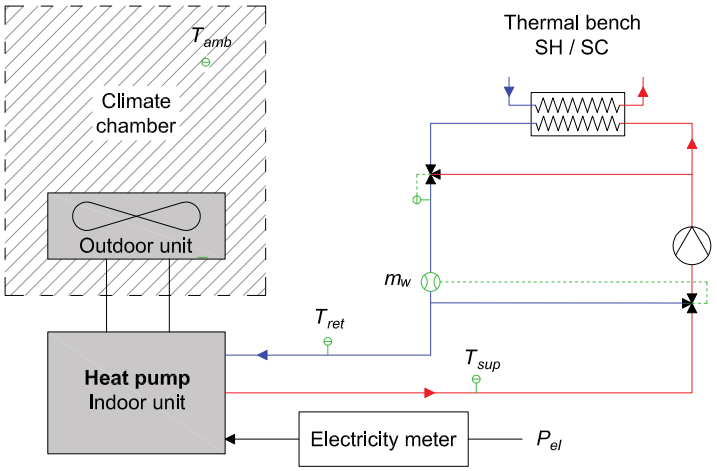

Figure 5. Experimental setup for the measurement of the static tests points.

Static tests were realized in an experimental setup to obtain data of the selected equipment, as shown in Figure 5. The device tested in the laboratory is a Hitachi Yutaki reversible air-to-water VSHP of nominal heating power 10 kW. The outdoor unit of the heat pump was placed in a climate chamber where the air temperature can be controlled in a range of -30°C to 40°C. The water circuit was connected to a thermal bench emulating the load, whether in heating or cooling mode.

2.3.1. Heating static tests

The following parameters were changed in their respective ranges for the static tests in heating mode: $T_{amb} \in \{-7°C; 2°C; 7°C; 12°C\}$, $T_{sup} \in \{35°C; 45°C; 55°C\}$ and $\Delta T \in [\![1°C, 8°C]\!]$. The ranges of T_{amb} and T_{sup} correspond to the standard test conditions found in standard EN 14511-2 [35], enabling to compare with the manufacturer's data.

For each experimental point, at least 30 minutes of data were recorded in steady state, after leaving 20 minutes of transition between one point and the next one. The measured parameters (T_{sup}, T_{ret}, $\dot{m}_w$, P_{el}, f, T_{amb}) were averaged over the measuring period. It was ensured that no defrost operation occurred during the measuring period, to avoid distorted measurements. The experimental points are presented in Figure 6. It is observed that at low load ($\Delta T \leq 3°C$), the heat pump is not able to modulate and exhibits an on-off cycling behavior that induces a low COP. At high load ($\Delta T \geq 6°C$) in some cases, the heat pump cannot reach the desired set-point despite the compressor running at full speed, and a low COP is also observed. The imperfect control of the air temperature in the climate chamber (standard deviation up to 2°C in some cases) also explains some of the observed deviations from the desired set-points. In the laboratory, the temperatures are measured with PT100 sensors that have a precision of ±0.25 K (thus for the temperature difference in the water loop, the precision is ±0.5 K). The induction flow meter for the measurement of the water flow has a high precision of ±0.2 to 0.5%, which makes it negligible, and the power measurement has a precision of ±1%.

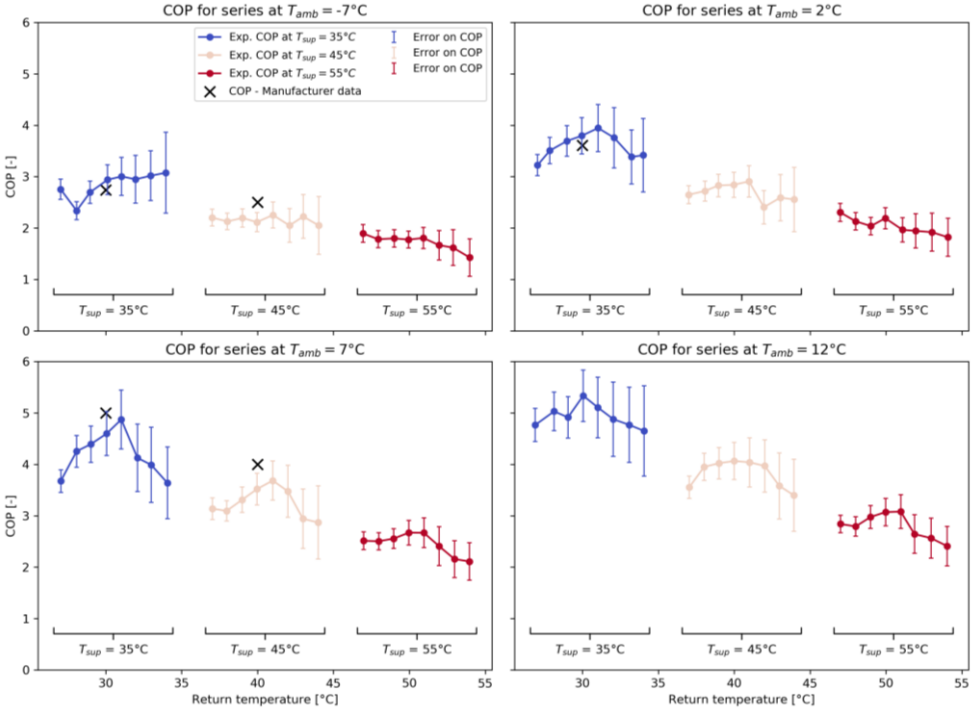

Figure 6. COP experimental points measured in the heating static tests, represented in function of T_{sup}, T_{ret} and T_{amb}. The manufacturer data (x markers) from the catalogue are also represented for comparison.

Two different models of the heat pump must be developed for the co-simulation framework: a detailed one to be used in TRNSYS (subscripted det), and a more simplified one for the MPC controller (subscripted $simpl$), as explained in section 2.1 and shown in Figure 1. Since the heat pump

cannot be controlled directly by deciding the frequency of the compressor (it is a 'hidden' internal parameter), this variable was discarded for fitting the models.

For the simplified model, only terms of T_{amb} and T_{sup} are chosen as inputs, as shown in Eq.(2).

$$P_{el,simpl} = \left[\frac{1}{COP}(T_{sup}, T_{amb})\right] \cdot Q = \left[a_0 + a_1 T_{sup} + a_2 T_{amb} + a_3 {T_{amb}}^2 + a_4 T_{sup} T_{amb}\right] \cdot Q \quad (2)$$

Since the only quantity that is of interest for the MPC objective is the inverse of the COP (later multiplied by the thermal power Q to obtain the electrical power P_{el}), it is this amount which is modelled. Furthermore, 1/COP presents a more linear behavior than the COP itself; a linear model can then be retrieved more easily. The least square method was employed to fit the models on the experimental data, and thus find the optimal values of the coefficients a_i which are presented in Table 2. The series of experimental points with $T_{amb} = -7℃$ was discarded to fit the model, since such low temperatures never occur in the considered climate for the dynamic simulations in which this model will be used. The model is therefore fitted around the operating conditions in which the heat pump is supposed to function, i.e. it was realized on 72 points. The obtained RMSE was 0.18 kW for the $P_{el,simpl}$ model (NRMSE = 6.4%). On Figure 7, the measured experimental data points are compared with the COP model of Eq.(2). The model does not offer a perfect representation of the data, however this result is considered sufficient given the restrictions of the linear model and the later use of this model. A similar model obtained from the literature [12] was also plotted on Figure 7 for comparison: a clear offset is visible since the heat pump presented in that study is a different model, but the same trend is conserved.

In previous literature [12], Verhelst et al. already discussed the formulation of the optimal control problem in terms of COP. They found that modelling the heat pump performance in function of (T_{sup}, T_{amb}) seems to perform almost as good as if the frequency of the compressor was additionally taken into account. However, in the present work, Eq.(2) would become non-linear if T_{sup} was kept as a variable in function of Q, and thus it would not be solvable in the current configuration. For this reason, it is chosen to consider constant supply temperatures when accounting for the heat pump performance. However, since the heat pump operates in two distinct modes (for space heating or DHW production), two different supply temperatures are assigned, which still enables to consider different efficiencies at two operating points. $T_{sup,SH,0} = 35℃$ since the heat pump operates at lower supply temperature in space heating, and $T_{sup,TES,0} = 55℃$ since the DHW must always be produced at high temperatures to keep the TES tank hot enough and avoid propagation of legionella. As a summary, in the MPC controller the electricity use of the heat pump for heating can be written as in Eq. (3):

$$P_{el,simpl,tot} = \left[\frac{1}{COP}(T_{sup,SH,0}, T_{amb})\right] Q_{SH} + \left[\frac{1}{COP}(T_{sup,TES,0}, T_{amb})\right] Q_{TES} \quad (3)$$

Considering Eq.(3) in its objective function, the MPC algorithm will determine the optimal values of Q_S and Q_{TES} over the prediction horizon. However, an additional equation is needed to obtain the actual values of T_{sup}, which is the actual variable sent to the "real" building (TRNSYS model). This equation represents the heat transfer between the water circuit of the heat pump and its load. For SH, it corresponds to the emitters which in this case are Fan Coil Units (FCU), and Eq. (4) is used. The coefficient M_S depends on the mass flow rate of the water circuit, the efficiency of the FCU and their ventilation rate. A regression on TRNSYS simulation data led to identify the coefficient $M_S = 0.222\ kW/K$. In the case of DHW, Eq. (5) is used and it corresponds to the tank charging. The coefficient $M_{TES} = 2.32\ kW/K$ is obtained considering the water flow rate and a fully efficient heat transfer between the two water circuits.

$$Q_S = M_S(T_{sup,S} - T_{int}) \quad (4)$$

$$Q_{TES} = M_{TES}(T_{sup,TES} - T_{TES}) \quad (5)$$

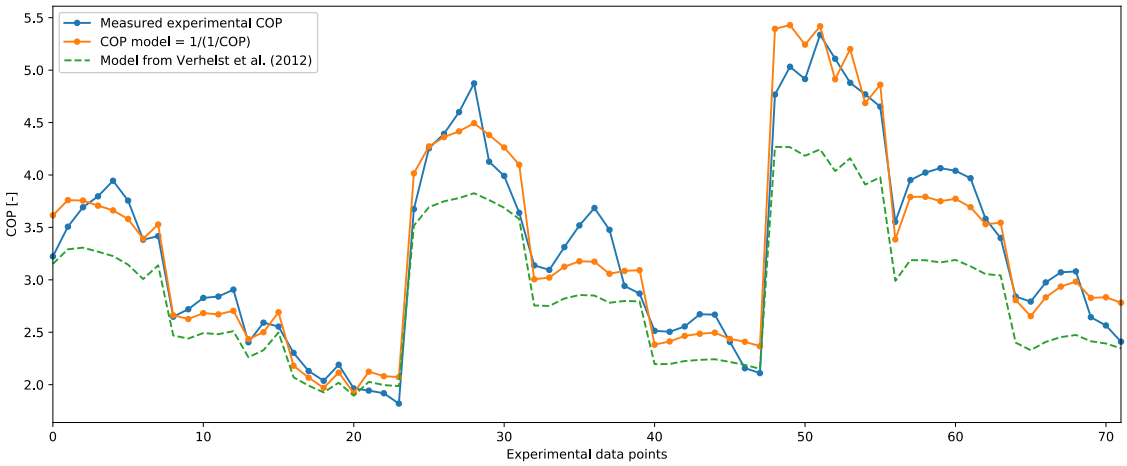

Figure 7. Comparison of the fitted simplified COP model with the experimental data and another model from the literature [12] (in heating mode).

Table 2. Obtained coefficients of the heat pump performance models in heating mode.

Simple model – Heating mode							
Coefficient	a_0	a_1	a_2	a_3	a_4		
Value	-0.09792	0.01056	0.00252	-0.00013	-0.00024		
Detailed model – Heating mode							
Coefficient	b_0	b_1	b_2	b_3	b_4	b_5	b_6
Value	-1.3128	0.00076	0.00786	0.6488	0.2678	-0.0381	0.2831

For the detailed model, there are no constraints of linearity like in the MPC simplified model, therefore it contains squared and bilinear terms. The fit is realized on the same data and with the same technique. The part-load ratio term is $PLR = Q/Q_{max}$, with $Q_{max} = 10\,kW$ chosen as the constant nominal capacity, since this capacity is always guaranteed independently of the operating conditions. The resulting equation is presented in Eq. (6) and the obtained coefficients b_i in Table 2. For the detailed $P_{el,det}$ model, RMSE = 0.121 kW and NRMSE = 5.46%, thus the improvement is relatively minor. This can be observed in Figure 8, where both the detailed and simplified models of P_{el} are represented against the corresponding experimental data. Small discrepancies are observed at the extreme low and high values of P_{el}.

$$P_{el,det} = b_0 + b_1 {T_{sup}}^2 + b_2 T_{amb} + b_3 PLR + b_4 Q + b_5 T_{amb} Q + b_6 PLR\, T_{amb} \quad (6)$$

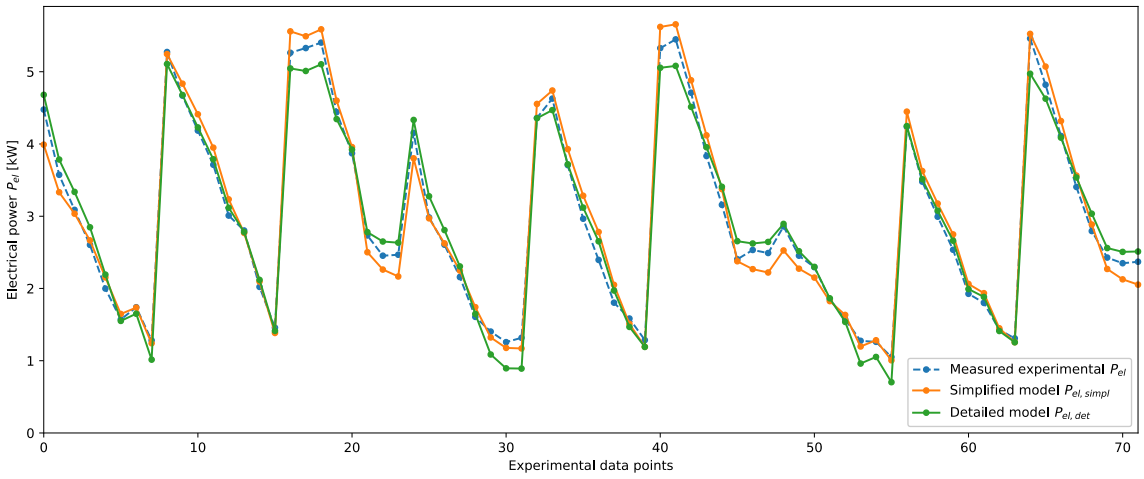

Figure 8. Comparison of the detailed and simplified P_{el} models with the experimental data (in heating mode).

2.3.2. Cooling static tests

A similar methodology was adopted for the cooling mode of the heat pump. In that case, the parameters for the experimental static tests were varied in the following ranges: $T_{amb} \in \{20°C; 25°C; 30°C; 35°C\}$, $T_{sup} \in \{7°C; 12°C; 18°C\}$ and $\Delta T \in [\![-8°C, -1°C]\!]$. The results of the data points in terms of EER (equivalent of COP for cooling) are represented in Figure 9. Contrary to the heating tests, it appears that the efficiency of the heat pump in cooling mode does not depend much on the outdoor temperature T_{amb}. Furthermore, a certain load ($|\Delta T| \geq 3°C$) is required for the heat pump to function at a higher efficiency, otherwise it will exhibit an on and off behavior, which produces start-up losses and deteriorates the overall EER.

The same methodology than in heating mode was applied to obtain a model of the quantity 1/EER. However, the fit obtained was not satisfactory, hence the electricity use P_{el} of the heat pump in cooling mode was directly modelled instead. The simpler model to be used by the MPC controller is presented in Eq. (7), while the more detailed formulation for the TRNSYS simulation is presented in Eq. (8). In these equations, Q_{SC} is the thermal cooling power (counted positive).

$$P_{el,simpl} = c_0 + c_1 T_{amb} + c_2 T_{sup,SC} + c_3 Q_{SC} \quad (7)$$

$$P_{el,det} = d_0 + d_1 T_{amb} + d_2 T_{sup,SC} + d_3 Q_{SC} b_0 + d_4 PLR + d_5 T_{sup,SC} Q_{SC}^2 + d_6 PLR\, Q_{SC}^2 \quad (8)$$

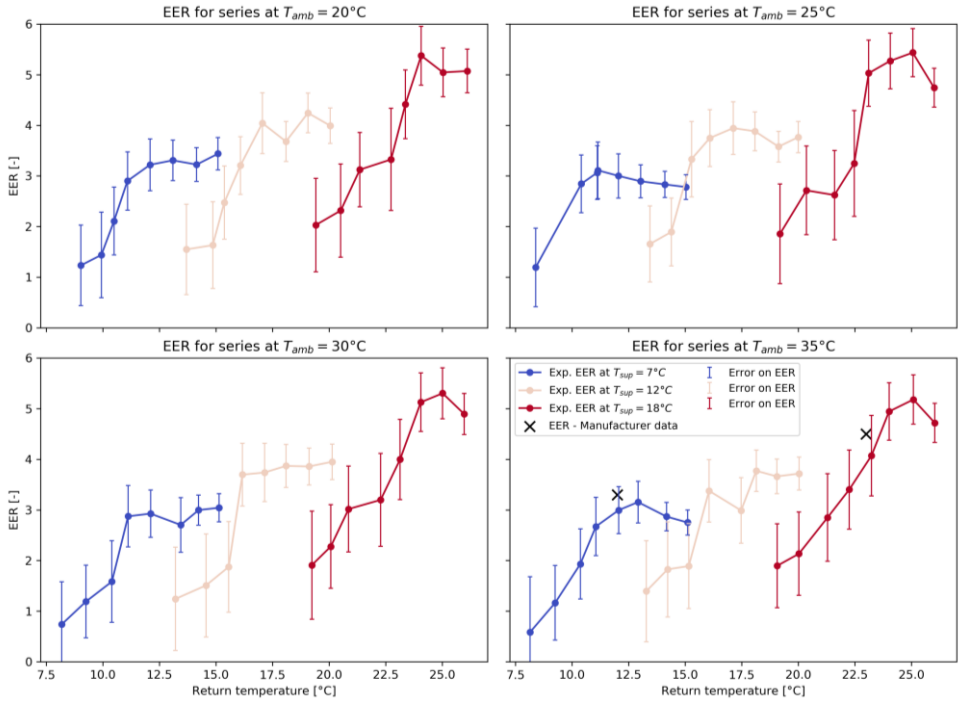

Figure 9. EER experimental points measured in the cooling static tests, represented in function of T_{sup}, T_{ret} and T_{amb}. The manufacturer data (x markers) from the catalogue are also represented for comparison.

The points chosen for the model identification are only the points with $|\Delta T| \leq 5°C$. The heat pump model is not suited for higher values of $|\Delta T|$ (it does not reach the desired set-point temperature in these cases), and furthermore, such high loads are not expected in the dynamic simulations in which the model will be used. The model fitting is thus realized on 60 points. After the least square method is applied, an RMSE value of 0.097 kW is obtained (NRMSE: 7.46%) for the simpler model. For the more detailed model, RMSE = 0.078 kW (NRMSE: 6.0%), therefore the gain in precision is relatively small. The optimal c_i and d_i coefficients are presented in Table 3. It can be noted that the coefficients c_1 and d_1, associated with the ambient temperature, are the lowest coefficients, confirming that this input parameter has little influence on the heat pump performance. The comparison between the models and the data points is presented in Figure 10. The simplified

model is considered satisfactory given its simplicity and despite the fact that the spikes of electricity consumption are not always captured, whereas the detailed model performs better at these points, as seen in Figure 10.

It should be noted that this model is only valid when the heat pump is turned on (approximately for values of $Q_{SC} \geq 2\ kW$). To obtain $P_{el,simpl} = 0\ kW$ when $Q_{SC} = 0\ kW$, the coefficients c_0, c_1 and c_2 must be multiplied by the on-off signal δ_S (see in section 2.5). To summarize, the simplified electricity use of the heat pump in cooling mode for the MPC is formulated in Eq.(9).

$$P_{el,simpl,tot} = \left[\left(c_0 + c_1 T_{amb}(k) + c_2 T_{sup,SC}\right) \cdot \delta_S(k) + c_3 Q_{SC}(k)\right] + \left[\frac{1}{COP}(T_{sup,TES}, T_{amb})\right] Q_{TES} \quad (9)$$

Table 3. Obtained coefficients of the P_{el} models in cooling mode.

Simple model – Cooling mode							
Coefficient	c_0	c_1	c_2	c_3			
Value	1.2313	0.0008	-0.0343	0.1486			
Detailed model – Cooling mode							
Coefficient	d_0	d_1	d_2	d_3	d_4	d_5	d_6
Value	1.0355	0.0007	-0.021	0.1902	-0.0527	-0.0009	0.0073

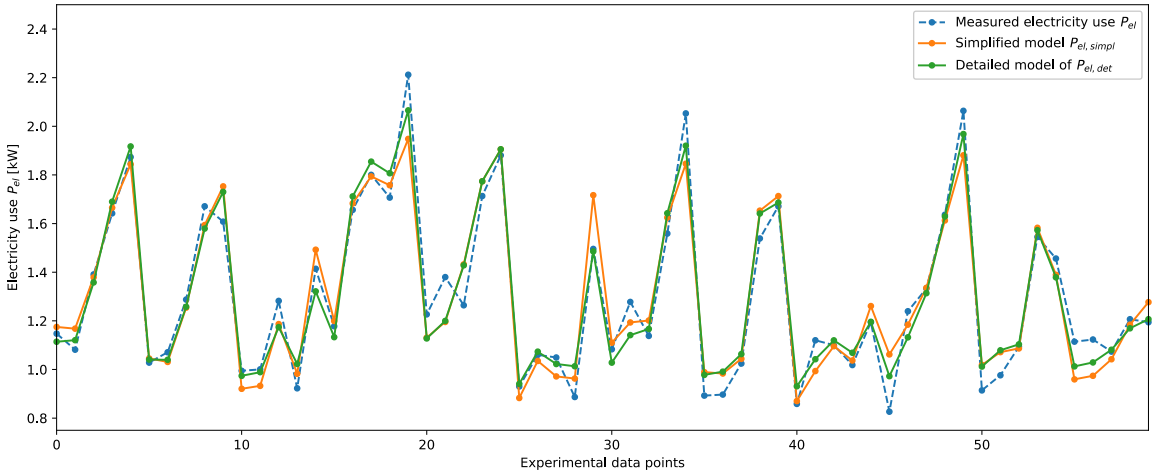

Figure 10. Comparison of the fitted P_{el} models with the experimental data points.

2.4. Model Predictive Control algorithm

The overall MPC control algorithm was developed to manage the heating and cooling of the building, and to exploit the flexibility of those flexible heat pump loads. The mathematical formulation of this problem is presented in Algorithm 1. The model was already described in section 2.2; the constraints and the objective function are clarified in the following subsections.

Algorithm 1 – Model Predictive Controller

Objective:

$$\min_{u,\delta} J = \left[\alpha_\varepsilon J_\varepsilon + \alpha_{\Delta u} J_{\Delta u} + (1 - \alpha_\varepsilon - \alpha_{\Delta u}) J_{obj}\right]$$

Subject to:

$\forall k \in [\![1, N]\!]$

Model:

$$\begin{cases} \boldsymbol{x}(k+1) = \boldsymbol{A} \cdot \boldsymbol{x}(k) + \boldsymbol{B_u} \cdot \boldsymbol{u}(k) + \boldsymbol{B_e} \cdot \boldsymbol{e}(k) \\ \boldsymbol{y}(k+1) = \boldsymbol{C} \cdot \boldsymbol{x}(k) \end{cases}$$

Constraints on the inputs:

$$\begin{cases} \delta_S(k) \cdot \underline{Q_S} \leq Q_S(k) \leq \delta_S(k) \cdot \overline{Q_S} \\ \delta_{TES}(k) \cdot \underline{Q_{TES}} \leq Q_{TES}(k) \leq \delta_{TES}(k) \cdot \overline{Q_{TES}} \\ \delta_S(k) + \delta_{TES}(k) \leq 1 \end{cases}$$

Constraints on the outputs:

$$\begin{cases} \underline{T_{int}}(k) - \varepsilon(k) \leq T_{int}(k) \quad (heating) \\ T_{int}(k) \leq \overline{T_{int}}(k) + \varepsilon(k) \quad (cooling) \\ \underline{T_{TES}} - \varepsilon(k) \leq T_{TES}(k) \qquad (\varepsilon \geq 0) \end{cases}$$

2.4.1. Constraints on the inputs

Continuous variables (i.e. the thermal powers Q_S and Q_{TES} delivered respectively to the building and the tank) were chosen as the inputs controllable by the MPC, to avoid including the heat emitter within the model. In order to switch from the space heating/cooling to the DHW production mode, it is however necessary to introduce the binary variables δ_S and δ_{TES}. They equal 1 when their respective mode is activated, 0 otherwise. The heat pump can only operate in one mode at a time, so the binary variables are constrained by $\delta_S(k) + \delta_{TES}(k) \leq 1$. Introducing binary variables transforms the nature of the control problem, and thus the MPC must resort to Mixed Integer Linear Programming (MILP) instead of simpler Linear Programming (LP) to solve it [36].

Such binary variables also enable to limit the heating power Q in a certain range $[\underline{Q}; \overline{Q}]$ when the heat pump is turned on. With only the continuous variables Q_S and Q_{TES}, the MPC could have decided to provide very low values of the heating power Q, without turning it off. In reality, a heat pump system has a minimum power below which it cannot operate; for instance with the considered equipment, the frequency of the compressor cannot drop below 31 Hz, if the load is still too low for that frequency the heat pump would switch off. The binary variables and the ranges of heating power enable to reproduce this behavior. The chosen ranges correspond to the manufacturers specifications and the range of operation observed in static tests: $\left[\underline{Q_{SC}}; \overline{Q_{SC}}\right] = [-8\ kW\ ;\ -2.5\ kW]$ in cooling mode, $\left[\underline{Q_{SH}}; \overline{Q_{SH}}\right] = [3\ kW\ ;\ 10\ kW]$ in heating mode, and $\left[\underline{Q_{TES}}; \overline{Q_{TES}}\right] = [10\ kW\ ;\ 10\ kW]$ in DHW production mode (DHW is always produced at full load of the heat pump).

2.4.2. Constraints on the outputs

For comfort reasons, additional constraints are set to the two outputs of the MPC controller. The internal zone temperature T_{int} must stay above the boundary $\underline{T_{int}} = 20℃$ in winter or below $\overline{T_{int}} = 26℃$ in summer. These constraints are relaxed with the slack variable ε: in this way, small excursions outside the hard constraints are permitted at a certain cost (see also next section 2.4.3). Regarding the tank storing DHW, its temperature T_{TES} must stay above $\underline{T_{TES}} = 50℃$ to avoid the spread of legionella. In fact, an additional anti-legionella protection (rising the temperature of the tank to 70°C for 10 minutes) is normally activated every week for more safety, but this feature is not studied in the present work since the considered simulations only last 3 days and the anti-legionella setting make use of an additional electrical resistance to reach 70°C, not the heat pump itself.

2.4.3. Objectives of the MPC

As seen in Algorithm 1, the MPC algorithm intends to minimize a certain objective over the prediction horizon. In the present case, the objective comprises in fact three aspects, weighted by the corresponding coefficients α:

- maintaining the comfort level with the objective J_ε, as shown in Eq. (10). In fact, it consists in limiting the discomfort, or in other words, avoid the excursions outside the defined temperature boundaries. ε is a slack variable that enables to soften the constraints on the output temperatures. In principle $\varepsilon = 0$, but exceptionally, the temperature is allowed to trespass the boundaries ($\varepsilon > 0$); the cost of this constraint violation is reflected in the objective

J_ε, as shown in Eq. (10). As another advantage, this formulation avoids infeasibility of the MPC in the case where the initial states are found outside the boundaries (which typically happens at start-up for instance, or due to discrepancies of the model when operating close to the boundaries).

$$J_\varepsilon = \sum_{k=1}^{N} \varepsilon(k) \tag{10}$$

- smoothing the control actions to avoid too frequent on-off switching with the objective $J_{\Delta u}$, as shown in Eq. (11).

$$J_{\Delta u} = \sum_{k=2}^{N} \|u(k) - u(k-1)\|_1 \tag{11}$$

- an actual objective J_{obj} which can be the minimization of the thermal energy delivered to the building J_{en}, the minimization of the cost of the electricity used by the heat pump for delivering this energy J_{cost}, or the minimization of the CO_2 emissions related to this electricity use J_{CO2}. The formulation of these objectives is detailed in the next section 2.5.

2.5. Tested MPC configurations

2.5.1. Thermal energy minimization (MPC ThEnerg)

In this configuration, the quantity minimized by the MPC over the control horizon is the thermal energy delivered to the building (in addition to the smoothing and discomfort terms), hence without taking into account the variable efficiency of the heat pump system. The mathematical formulation with $J_{obj} = J_{en}$ is written in Eq. (12):

$$J_{en} = \sum_{k=1}^{N} \|u(k)\|_1 = \sum_{k=1}^{N} [Q_S(k) + Q_{TES}(k)] \tag{12}$$

In the overall objective of the MPC, J_{en} is combined with two other objectives (comfort and smoothing of the control). To determine the weighting coefficients α between these different quantities, Pareto fronts are plotted, where several values of the coefficients are tested on simulations. The results are plotted separating the different components of the objective function, as can be seen in Figure 11. In this graph, the J_ε objective is represented on the y-axis, J_{en} on the x-axis, and $J_{\Delta u}$ through color mapping of the points. The different lines correspond to different values of $\alpha_{\Delta u}$, while the different points of a line correspond to different values of α_ε.

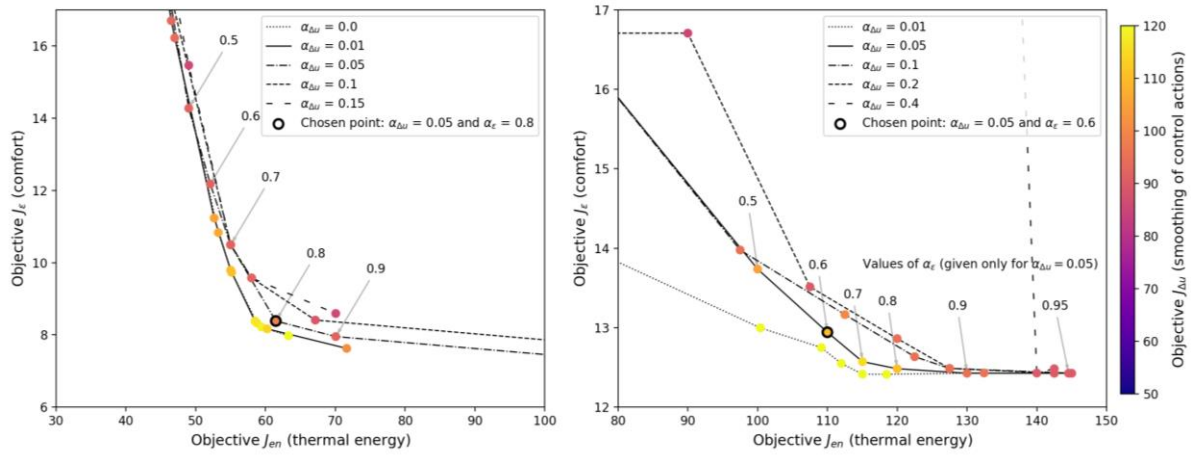

Figure 11. Pareto fronts for the J_{en} objective, in the heating (left) and cooling (right) modes.

To choose appropriate values of the weighting coefficients, one must remain in the right horizontal part of the lines, where the discomfort J_ε is at its minimum. At the same time, it is preferable to minimize the thermal energy J_{en}, therefore to stay as much on the left of the graph as

possible. Furthermore, one must also avoid unreasonably high computation times and high values of $J_{\Delta u}$ (yellow colors on the present graph), even though this is the least relevant parameter (with time steps of 12 minutes, a cyclic on-off behavior would not cause many problems). As a compromise between all these considerations, the values chosen are $\alpha_{\Delta u} = 0.05$ and $\alpha_{\varepsilon} = 0.8$ for the J_{en} objective in heating mode; $\alpha_{\Delta u} = 0.05$ and $\alpha_{\varepsilon} = 0.6$ in cooling mode. The same approach is repeated for every MPC configuration.

2.5.2. Cost minimization (MPC Cost)

In this configuration, the cost of the electricity used by the heat pump is minimized by the MPC. This configuration presents an increased complexity, since the electricity use is introduced in the equation (and not only the delivered heat as previously), and therefore the heat transmission by the emitter and the performance of the heat pump must both be taken into account into the objective function. For this purpose, the simplified models detailed in section 2.3 are utilized.

The electricity used by the heat pump is then multiplied at every time step by a time-varying cost of electricity E_{el} (in €/MWh, changing every hour), normalized by $E_{el,max}$. In the present case, the voluntary price for small consumers (PVPC in Spanish) is used: it is an available tariff for consumers of less than 10 kW contracted power in Spain, which historical data and forecasts are public [37]. Introducing such a penalty helps the decision-making process of the MPC since it already predefines favorable or non-favorable periods for when to operate the systems. It should be noted that the other costs of the building (notably related to the energy use of the FCU fans) are not included in the cost objective J_{cost}, since they would not influence the calculation of the optimal MPC plan (constant energy use when the FCU are on). The formulation with $J_{obj} = J_{cost}$ differs in heating (Eq. (13)) and in cooling (Eq.(14)). The Pareto fronts for J_{cost} are presented in Figure 12. In this configuration, the chosen values are $\alpha_{\Delta u} = 0.01$ and $\alpha_{\varepsilon} = 0.15$ for cooling, $\alpha_{\Delta u} = 0.01$ and $\alpha_{\varepsilon} = 0.5$ for heating.

$$J_{cost} = \sum_{k=1}^{N} \left[P_{el,SH}(k) + P_{el,TES}(k)\right] \cdot \frac{E_{el}(k)}{E_{el,max}} \tag{13}$$

$$= \sum_{k=1}^{N} \left[\frac{1}{COP}\left(T_{sup,S}, T_{amb}(k)\right) \cdot Q_S(k) + \frac{1}{COP}\left(T_{sup,TES}, T_{amb}(k)\right) \cdot Q_{TES}(k)\right] \cdot \frac{E_{el}(k)}{E_{el,max}}$$

$$J_{cost} = \sum_{k=1}^{N} \left[P_{el,SC}(k) + P_{el,TES}\right] \cdot \frac{E_{el}(k)}{E_{el,max}} \tag{14}$$

$$= \sum_{k=1}^{N} \left[\left(c_0 + c_1 T_{amb}(k) + c_2 T_{sup,SC}\right) \cdot \delta_S(k) + c_3 Q_S(k) + \frac{1}{COP}\left(T_{sup,TES}, T_{amb}(k)\right) \cdot Q_{TES}\right] \cdot \frac{E_{el}(k)}{E_{el,max}}$$

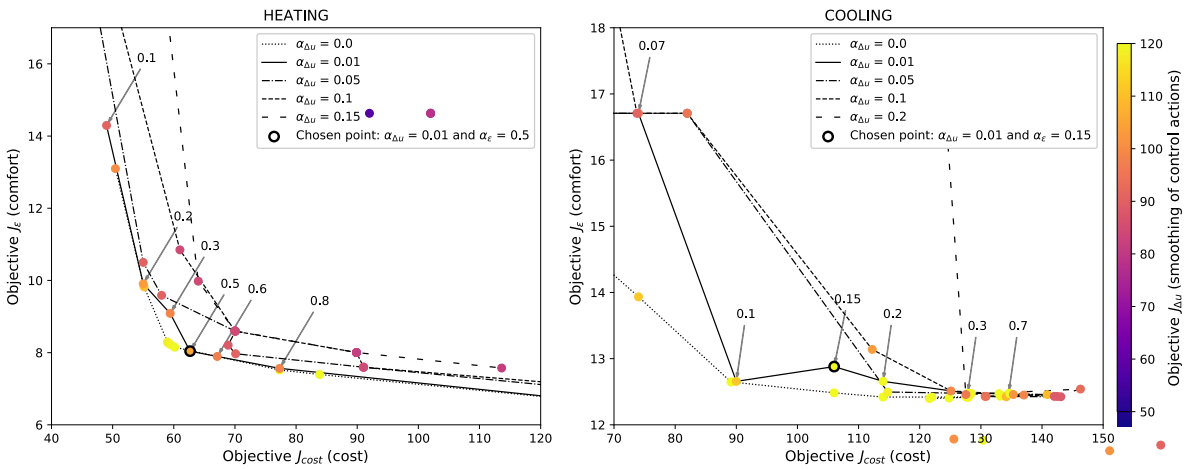

Figure 12. Pareto fronts for the J_{cost} objective, in the heating (left) and cooling (right) modes.

2.5.3. CO_2 emissions minimization (MPC CO_2)

This formulation resembles the previous J_{cost}, except that the monetary cost E_{el} is replaced by a cost in terms of CO_2 emissions E_{CO2} (in $kgCO_2/kWh$). For E_{CO2}, the marginal emissions factor (MEF) is used. This parameter estimates the emissions savings that can be realized from a change in the load (i.e. a demand response action), given the state of the electrical grid. It differs from the average emissions factor since it considers the supposed merit order in which the different sources of electricity generation are activated. The MEF is computed for every hour according to the model and calculations described in [15]. The formulation with $J_{obj} = J_{CO2}$ is presented in Eq. (15) (heating) and Eq. (16) (cooling). The Pareto curves for J_{CO2} are plotted on Figure 13. In this configuration, the chosen values are $\alpha_{\Delta u} = 0.05$ and $\alpha_{\varepsilon} = 0.15$ for heating, $\alpha_{\Delta u} = 0.01$ and $\alpha_{\varepsilon} = 0.15$ for cooling.

$$J_{CO2} = \sum_{k=1}^{N} \left[P_{el,SH}(k) + P_{el,TES}(k)\right] \cdot \frac{E_{CO2}(k)}{E_{CO2,max}} \tag{15}$$

$$= \sum_{k=1}^{N} \left[\frac{1}{COP}\left(T_{sup,S}, T_{amb}(k)\right) \cdot Q_S(k) + \frac{1}{COP}\left(T_{sup,TES}, T_{amb}(k)\right) \cdot Q_{TES}(k)\right] \cdot \frac{E_{CO2}(k)}{E_{CO2,max}}$$

$$J_{CO2} = \sum_{k=1}^{N} \left[P_{el,SC}(k) + P_{el,TES}(k)\right] \cdot \frac{E_{CO2}(k)}{E_{CO2,max}} \tag{16}$$

$$= \sum_{k=1}^{N} \left[\left(c_0 + c_1 T_{amb}(k) + c_2 T_{sup,SC}\right) \cdot \delta_S(k) + c_3 Q_S(k) + \frac{1}{COP}\left(T_{sup,TES}, T_{amb}(k)\right) \cdot Q_{TES}\right] \cdot \frac{E_{CO2}(k)}{E_{CO2,max}}$$

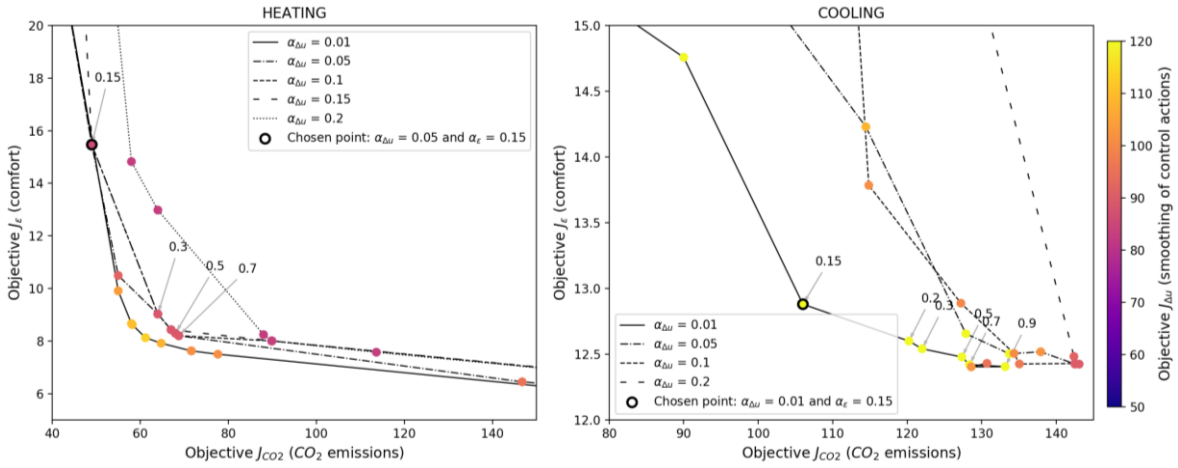

Figure 13. Pareto fronts for the J_{CO2} objective, in the heating (left) and cooling (right) modes.

2.5.4. Other parameters

Table 4. Summary of the utilized weighting coefficients.

Mode	**Heating**			**Cooling**		
Objective	J_{en}	J_{cost}	J_{CO2}	J_{en}	J_{cost}	J_{CO2}
Value of α_{ε}	0.8	0.5	0.15	0.6	0.15	0.15
Value of $\alpha_{\Delta u}$	0.05	0.01	0.05	0.05	0.01	0.01
Value of $\alpha_{obj} = (1 - \alpha_{\varepsilon} - \alpha_{\Delta u})$	0.15	0.49	0.8	0.35	0.84	0.84

All the weighting coefficients are summarized in Table 4, and it can be seen that the values differ between heating and cooling, similarly than for the low order RC models. Among the other parameters intervening in the MPC configuration, the time horizon was chosen as 24 hours ahead, i.e. $N = 120$ time steps of 12 minutes. Choosing this value for the prediction horizon enables to capture the daily patterns occurring in the occupancy, weather and grid status evolutions. It was

shown in [17] that 24h is the most common prediction horizon for MPC in buildings; longer horizons might be better suited if the time constant of the building is large (e.g. TABS applications), but are not necessary otherwise. The discretization time step for the MPC is chosen as 12 minutes: in this way, the heat pump must stay ON or OFF for at least this duration, reflecting the minimum up or down time usually set in the internal controller of a heat pump. Oscillations at a too high frequency would in fact damage the machine in the long term. Furthermore, a time step of 12 minutes captures the dynamics of the building with sufficient accuracy and represents a satisfactory trade-off. In the detailed TRNSYS simulation on the other hand, a finer resolution of 3 minutes is chosen, so as to better observe the intrasampling behavior of the systems within one control action.

2.5.5. Boundary conditions and scenarios tested

All the tested scenarios consist of 3 days in the winter (24 to 26th of February 2018) and summer season (8 to 10th of July 2016). These periods were chosen because they present the following characteristics: high heating/cooling load, variety of weather conditions (cloudy and sunny days among the three days), sufficient variations in the input signals (especially the emissions signal). The occupancy patterns show some level of stochasticity between the different days (as shown later in sections 3.1 and 3.2), therefore it is considered that simulations of three days are sufficient for the scope of the present work.

The weather parameters necessary for the simulations were retrieved from a weather station located in Tarragona, Spain: ambient temperature, relative humidity, solar irradiation, wind direction and velocity. The price of electricity was retrieved from the Spanish Distribution System Operator website [37], and the CO_2 marginal emissions factor was calculated from data also originating from the same source. It should be noted that in the present work, the forecasts used by the MPC are perfect, meaning that the actual measured parameters are used as the prediction of the future.

3. Results

3.1. Heating cases

The boundary conditions and the reference case for heating are presented in Figure 14. In that reference case, the heat pump operation is managed by a simple thermostat controlling the zone temperature T_{int}. The set-point in winter is 21°C with a symmetric deadband of ±1°C, which means the lower temperature bound is 20°C, as for the MPC cases. In the following sections, the MPC strategies are analyzed under the angles of the selected KPIs.

It can firstly be observed in Figure 14 why the MEF CO_2 signal is preferred to the average EF: it follows the same trend, but its varies with larger amplitude, which represents an advantage for facilitating the optimization calculation of the MPC. The price signal displays a clear day-night pattern, with high price during the peak hours of the grid (afternoons) and low price at night. The price and CO_2 MEF signals show in general an opposite behavior, the peaks of the first one coinciding with the valleys of the other and vice versa. In the reference case, the heating loads predominate at night when the outdoor temperature is coldest, which constitutes a favorable situation with regards to the price signal, less so for the CO_2 MEF signal. Over the three winter days of that case, the heat pump uses 32.6 kWh of electricity which correspond to a cost of 3.26 € and average emissions of 8.99 $kgCO_2$.

In the top two graphs of Figure 14, the high and low penalty periods are highlighted by different background colors, whether the considered penalty signal is the price or the CO_2 emissions. The low and high thresholds of the two signals are defined by the 40th and 60th percentiles of the data for the next day define respectively, as studied in the parametric analysis of [39].

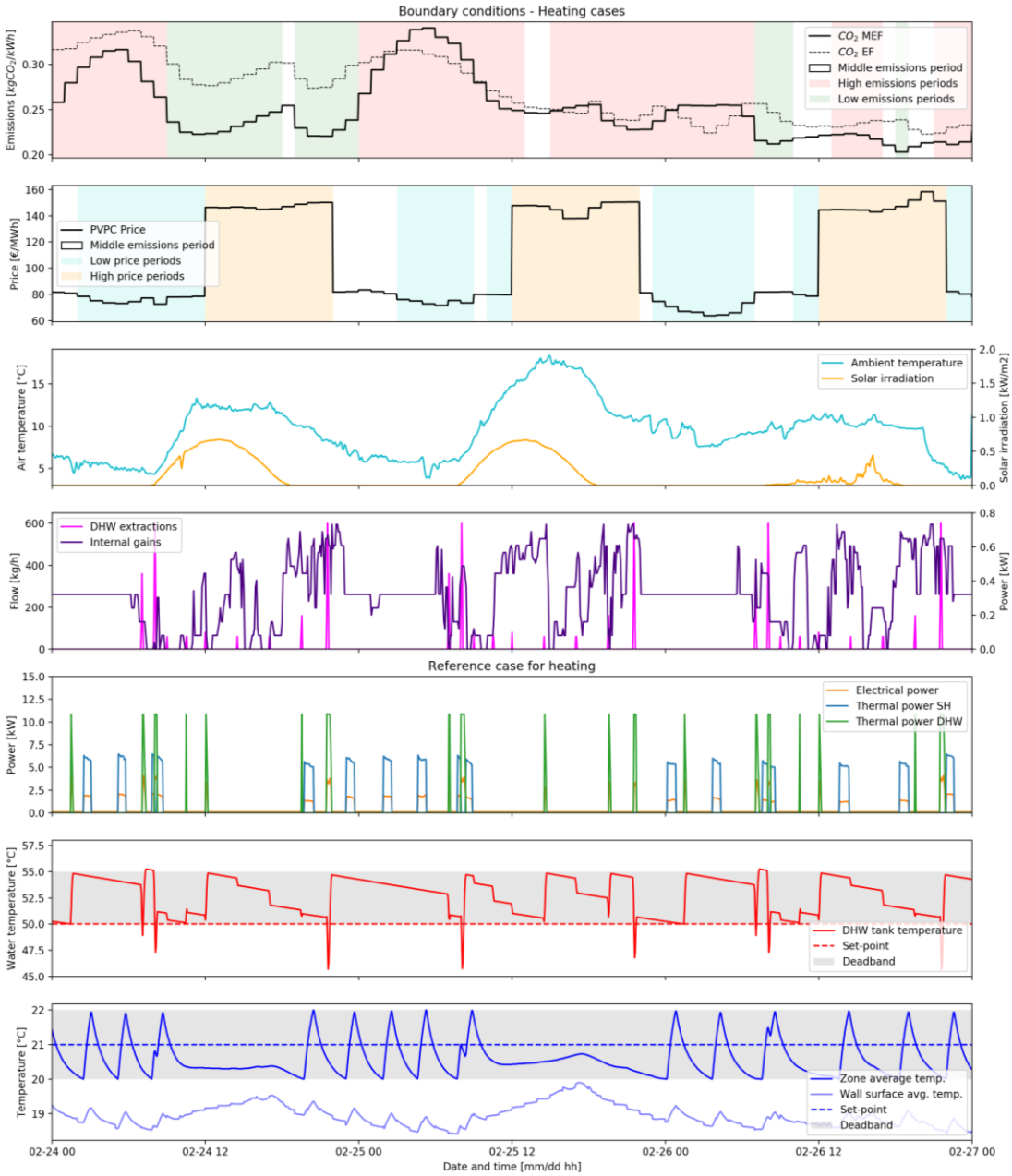

Figure 14. Boundary conditions and reference heating case. The first four graphs display the boundary conditions: CO_2 emissions and price signals, weather parameters and DHW extractions profile. The last three graphs show the reference heating case: the electrical and thermal powers of the heat pump, the resulting temperature in the TES tank and in the dwelling.

3.1.1. Flexibility factors

One major goal of implementing energy flexibility control strategies consists in shifting the loads towards periods of lower electricity price or lower CO_2 emissions from the grid. To quantify this shifting, the flexibility factor (FF) as defined in [38] is utilized. This indicator is calculated both with regards to the electricity price (FF_{cost}) and the CO_2 marginal emissions input signal (FF_{CO2}). The generic formulation is shown in Eq. (17), p referring to the penalty signal being used (price or emissions); with hp and lp respectively the high and low penalty periods. FF varies between -1 (all the electricity use of the heat pump occurs during hours of high price/emissions) and 1 (all the electricity use of the heat pump occurs during hours of low price/emissions).

$$FF_p = \frac{\int_{lp} P_{el}dt - \int_{hp} P_{el}dt}{\int_{lp} P_{el}dt + \int_{hp} P_{el}dt} \quad (17)$$

The flexibility factors are presented in Figure 15. As previously analyzed, the reference case benefits more from the price signal than from the CO_2 signal in heating mode: for that case, $FF_{cost} = 0.19$ and $FF_{CO2} = -0.42$. The low values of FF_{CO2} are also caused by the fact that the amount of high CO_2 MEF hours is larger than the amount of high price hours (see Figure 14). As expected, the case MPC Cost increases FF_{cost} the most, since this is its main objective: it reaches the value $FF_{cost} = 0.44$, while its $FF_{CO2} = -0.44$ is further degraded compared to the reference case. The results of the MPC CO_2 case are less satisfactory in terms of flexibility factors. This case fails to increase significantly the value of FF_{CO2} and thus to achieve its declared objective: $FF_{CO2} = -0.34$, at a similar level than MPC ThEnerg. This could be due to the low variations of the penalty signal in this case, which complicates the optimization process. Analyzing solely the flexibility factors, the MPC Cost configuration appears like the most efficient control strategy to achieve load-shifting.

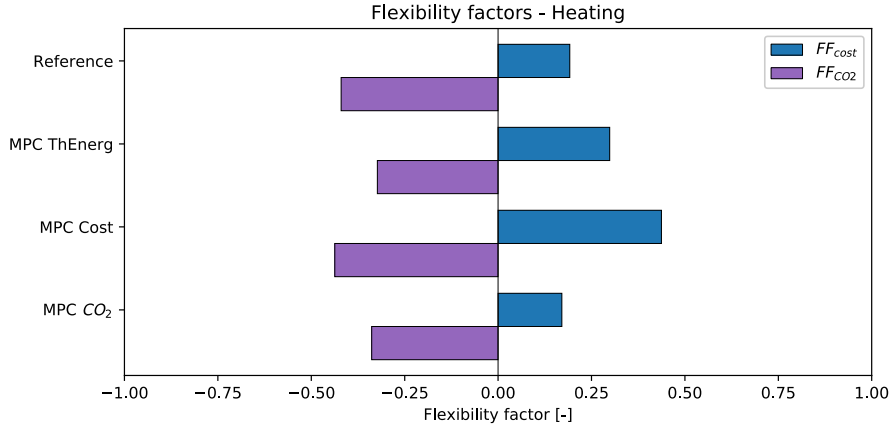

Figure 15. Flexibility factors of the studied heating cases, both in terms of cost and marginal CO_2 emissions.

3.1.2. Electrical and thermal energy

To understand how the MPC strategies affect the operation and efficiency of the systems, it is important to analyze the energy balance of the heat pump. In this regard, the delivered thermal energy $Q_{SH} + Q_{TES}$ (whether in space heating or DHW production mode) is calculated, as well as the overall electricity use of the heat pump during the three days of the analyzed cases, including a standby power of 95 W when the compressor is off (as measured with the real heat pump system in a laboratory setup). The ratio between these energy quantities represent the overall coefficient of performance of the system.

Furthermore, when analyzing the thermal energy balance over the simulation period, it is important to consider the energy stored or discharged within the building. In fact, if we consider the building and its water tank as storage elements, their state of charge is not equal at the beginning and at the end of the simulation, and this energy gap must be taken into account in the overall energy balance analysis. For this reason, we define the energy difference ΔE between the initial and final moments for the three states, as shown in Eq.(18).

$$\Delta E = C_{int}\left(T_{int,init} - T_{int,fin}\right) + C_w\left(T_{w,init} - T_{w,fin}\right) + C_{TES}\left(T_{TES,init} - T_{TES,fin}\right) \quad (18)$$

All the energy balance parameters are represented for each analyzed case in Figure 16. It is observed that for every MPC case, the thermal energy produced by the heat pump is slightly larger than the reference case, although the electrical energy use is lower, which results in a higher efficiency. The MPC controller usually chooses to operate the heat pump at a lower supply temperature, which means a higher COP of the heat pump, as shown previously in Figure 6. This

result already proves the benefits of choosing an MPC controller: by operating the system at a higher COP, the heat pump actually becomes a more sustainable option (the European Union notably considers electrically-driven heat pumps as a renewable energy option only if their seasonal COP surpasses a value of 2.5 [40]). This corroborates the findings of [41]. DHW is always produced with a supply temperature of around 55°C, therefore the COP during the tank charging operation would take lower values (in a range from 2 to 3 as seen in Figure 6). This naturally affects the overall COP of the system, as well as the standby losses which are not considered in the static tests or by the manufacturer data, where the heat pump only operates in steady-state conditions.

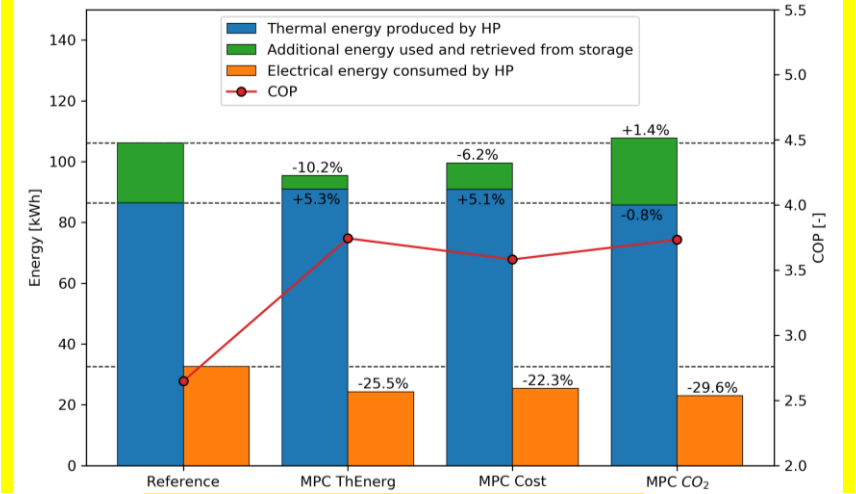

Figure 16. Energy analysis of the heating cases.

3.1.3. Cost and emissions

The actual outputs of the energy flexibility strategies can be measured in terms of monetary savings or CO_2 emissions avoided. These metrics are presented in Table 5, as savings compared to the reference case. For this reason, the choice of the reference case is crucial: in the present work, a simple thermostatic case was chosen as the reference since it is the most common type of controller. The monetary cost represents the money spent on the electricity use of the heat pump, but it does not include the other loads of the dwelling, nor the other parts of the electricity bill (e.g. taxes or grid connection fees).

If analyzing only the thermal energy produced by the heat pump, it appears that the case MPC ThEnerg does not achieve its minimization objective: it is in fact increased by 5.3% compared to the reference case. However, when considering the total energy use (hence also the energy ΔE retrieved from the storage), MPC ThEnerg presents the lowest value among the MPC cases, a reduction of 10.2% compared to the reference case. It retrieves less energy from the storage than the other cases, to preserve it and to minimize the overall energy use in the long term.

For a more detailed cost analysis, Figure 17 is plotted. On the top graph, the electricity use of the reference case and the MPC Cost case (the most relevant when analyzing the cost savings) are represented, highlighting the periods where the electricity price is higher. Even though the reference case already uses little electricity during these periods, a certain load shifting can be observed, as the MPC controller tends to avoid them to operate the systems. As a result, a "rebound effect" can sometimes occur when the high price period terminates: the system then needs to compensate for a prolonged reduced operation by turning the system on when the price becomes low again. A pre-heating effect also happens on the last day of the simulation: since on that day the solar radiation and the outside temperature are particularly low (see in Figure 14), the MPC controller anticipates the consequent increased heating needs combined with the high price, and decides to pre-heat the building when the price is still low. In this regard, the MPC controller behaves as expected. The bottom graph of Figure 17 presents the cumulated costs of all the analyzed cases: the three MPC cases perform better than the reference case and display a very similar behavior among them.

Table 5. Savings of the heating MPC cases in terms of cost and CO_2 marginal emissions.

MPC objective case		MPC ThEnerg	MPC Cost	MPC CO_2
Cost variation compared to the reference case	**[€]**	-0.91	-0.92	-0.98
	[%]	-27.9%	-28.1%	-29.9%
Thermal energy use J_{en} compared to the reference case	**[kWh]**	+4.59	+4.44	-0.67
	[%]	+5.31%	+5.14%	-0.78%
Energy difference between initial and final state ΔE	**[kWh]**	4.4	8.7	22.0
Total energy $(J_{en} + \Delta E)$ variation compared to the reference case	**[kWh]**	-10.8	-6.6	+1.5
	[%]	-10.2%	-6.2%	+1.4%
Electricity use variation compared to the reference case	**[kWh]**	-8.33	-7.27	-9.67
	[%]	-25.5%	-22.3%	-29.6%
Average CO_2 emissions variation compared to the reference case	**[kgCO_2]**	-2.41	-2.21	-2.79
	[%]	-26.8%	-24.6%	-31.1%
Marginal CO_2 emissions variation compared to the reference case	**[kgCO_2]**	-2.31	-2.03	-2.64
	[%]	-25.7%	-22.6%	-29.4%

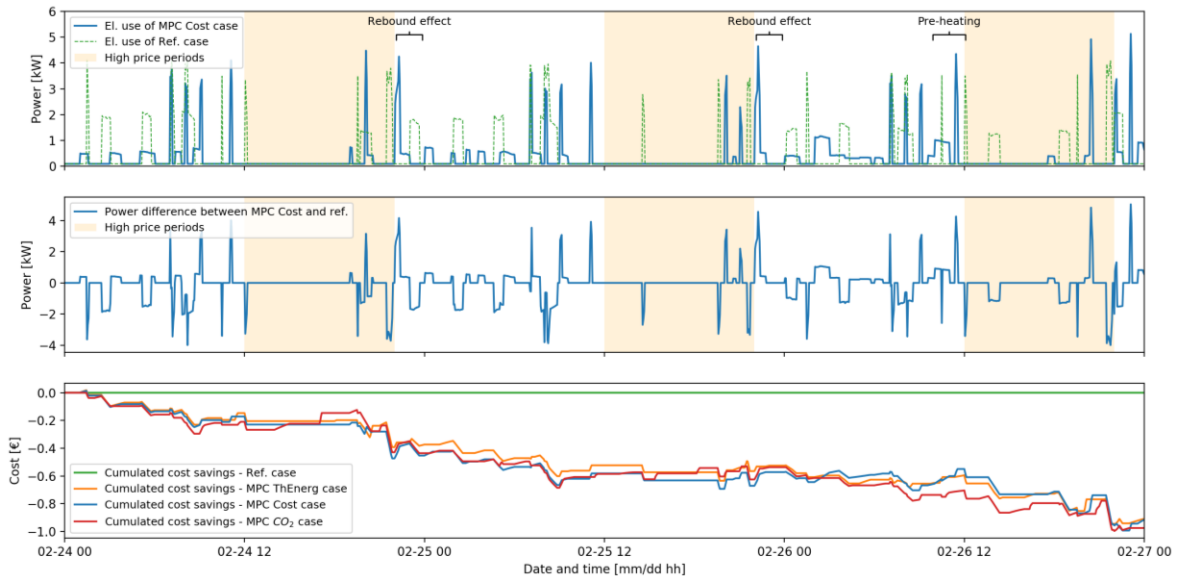

Figure 17. Electricity use of the heat pump in the reference and the MPC Cost cases (top graph), resulting difference (middle graph) and cumulated cost savings of the four studied cases (bottom graph).

For a more detailed analysis of the CO_2 emissions savings, Figure 18 is plotted. On the top graph, the electricity use of the reference case and the MPC CO_2 case (the most relevant when analyzing the emissions savings) are represented, highlighting the periods where the marginal emissions are higher. The expected load shifting towards periods where the grid emits less CO_2 is less clearly visible than in the MPC Cost case previously analyzed. In fact, the input signal of the CO_2 marginal emissions becomes almost flat during the second half of the experiment (see Figure 14): this could have complicated the optimization task of the MPC in this configuration. However, emissions savings are still achieved in all MPC cases, but they are mainly due to the operation of the heat pump at a lower supply temperature (i.e. at a higher efficiency), reducing the overall electrical energy used by the systems. Among them, MPC CO_2 logically yields the highest marginal emissions savings: -2.64 kgCO_2 (-29.4%). Table 5 also reveals that the average emissions calculation slightly underestimates the benefits compared to the marginal emissions calculation, although the two methods give close results. The MEF signal is still preferred as an input signal for its variations of larger amplitude.

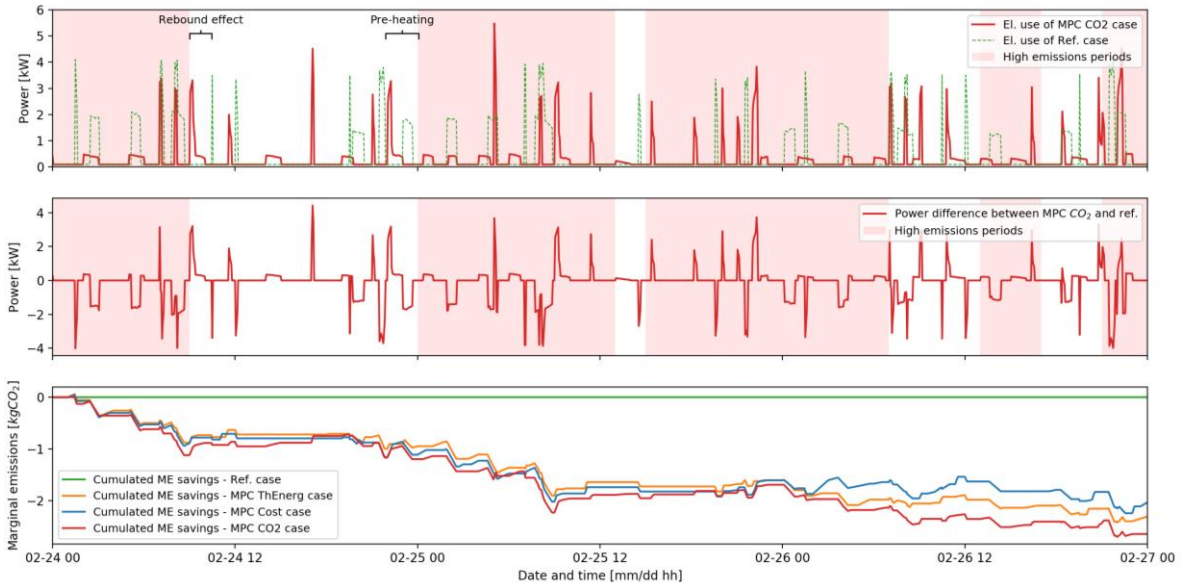

Figure 18. Electricity use of the heat pump in the MPC CO_2 and reference cases (top graph), resulting difference (middle graph) and cumulated marginal emissions savings of the four cases (bottom graph).

3.1.4. Comfort

The comfort of the occupants is of utmost importance when interfering with the control of the HVAC systems. To ensure acceptability of the users, the flexibility control strategies must not jeopardize their thermal sensations [4], [42]. For this reason, the resulting indoor temperature T_{int} is analyzed, in terms of time spent in the comfort categories defined by the standard EN 15251 [43]. It should be noted that thermal comfort is a much more complex topic, and that it depends on many other parameters (humidity, air velocity, activity level). However, the indoor temperature remains the most significant parameter and the easiest to analyze, therefore it provides meaningful insights about the thermal comfort. Figure 19 reveals that all the cases present similar comfort conditions than the reference cases, with a majority of the time spent in Cat.II (between 20 and 21°C), which is logical given the lower boundary of 20°C. Case MPC CO_2 presents a slight degradation of comfort, with incursions in the lowest acceptable comfort category (Cat. III: operative temperature between 18 and 20°C in the heating season), but Cat. IV (less than 18°C) is however never reached.

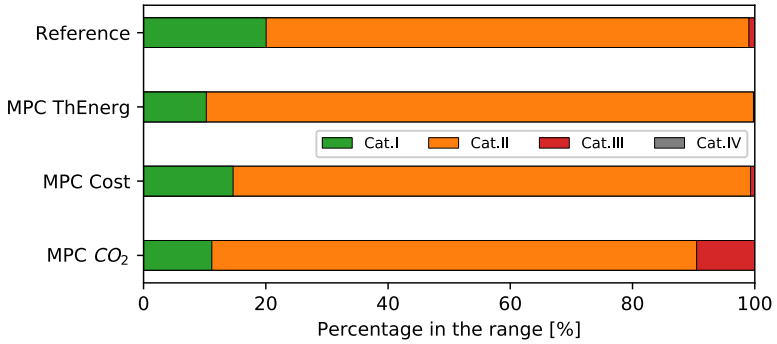

Figure 19. Comfort analysis of the heating cases.

3.2. Cooling cases

The boundary conditions and the reference case for cooling are presented in Figure 20. For the reference case, the set-point of the thermostat is fixed to 25°C, with the deadband of ±1°C, so that the upper bound is 26°C, as in the MPC cases. The MPC strategies are then analyzed in the following sections under the angles of the same KPIs than the heating cases. In the cooling season, the symmetric behavior of the two input signals (see the two top graphs of Figure 20) is accentuated:

765 during daytime where solar energy takes up a large part of the electricity production, the marginal
766 emissions are low while the price is high, following the same pattern than in winter. Conversely at
767 night, the price is low while the marginal emissions are high due to the use of more polluting energy
768 sources. Furthermore, in summer the cooling loads are concentrated in the afternoon due to high
769 solar heat gains entering the buildings, therefore the cooling configuration represents a more
770 favorable situation with regards to the reduction of emissions rather than the costs. Over these three
771 summer days, the heat pump uses 31.1 kWh of electricity corresponding to a cost of 2.78 € and
772 average emissions of 7.29 $kgCO_2$.
773

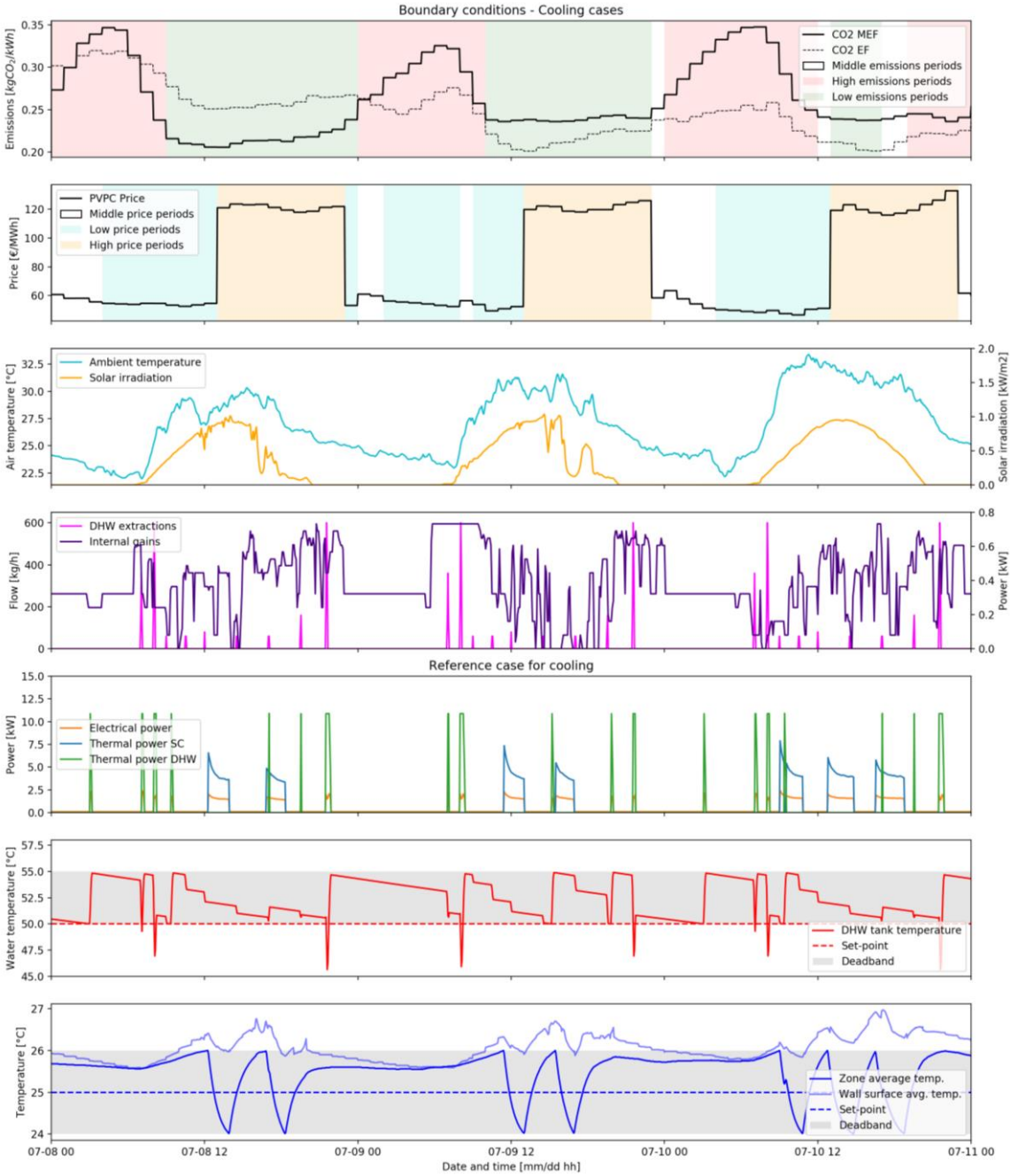

774
775 **Figure 20**. Boundary conditions and reference cooling case. The first four graphs display the boundary
776 conditions: CO_2 emissions and price signals, weather parameters and DHW extractions profile. The last three
777 graphs show the reference cooling case: the electrical and thermal powers of the heat pump, the resulting
778 temperature in the TES tank and in the dwelling.
779

3.2.1. Flexibility factors

As previously mentioned, the reference case in the cooling season presents more favorable characteristics for the reduction of CO_2 emissions than for the reduction of costs, according to the respective input penalty signals. As a result, $FF_{CO2} = 0.28$ while $FF_{Cost} = -0.20$ in that base case. When implementing the MPC Cost strategy, the FF_{Cost} increases significantly to reach a value of 0.27, which confirms the effectiveness of this configuration. MPC CO_2 only improves FF_{CO2} by +0.06: since it is already relatively high in the reference case, the margin for improvements is greatly limited.

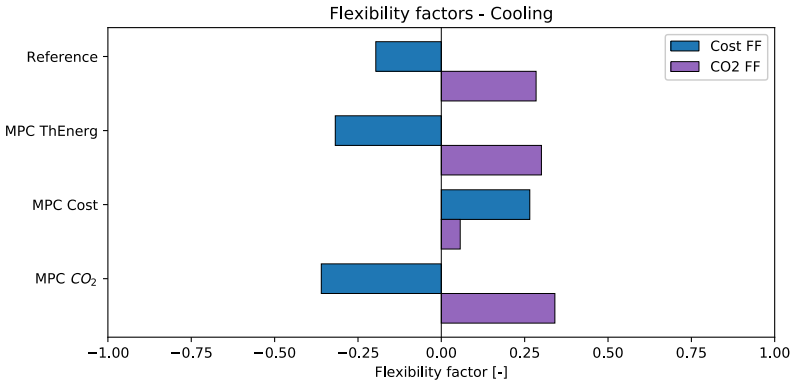

Figure 21. Flexibility factors of the studied cooling cases, both in terms of cost and CO_2 emissions.

3.2.2. Electrical and thermal energy

In cooling mode, the definitions need to be slightly adapted: since the thermal energy delivered to the space Q_{SC} is negative, the total energy considered is calculated as $|Q_{SH}| + Q_{TES}$. Dividing this quantity by the total electricity use of the heat pump over the three days duration gives the overall COP of the systems. The definition of ΔE must also be slightly updated: in cooling mode, a lower temperature corresponds to a higher state of charge while it is the opposite in heating mode, therefore minus signs are included, as shown in Eq.(19).

$$\Delta E = -C_{int}\left(T_{int,init} - T_{int,fin}\right) - C_w\left(T_{w,init} - T_{w,fin}\right) + C_{TES}\left(T_{TES,init} - T_{TES,fin}\right) \quad (19)$$

As observed in Figure 22, all configurations reduce the amount of thermal energy produced by the heat pump, while their electricity use remains at the same level, which causes a small drop in COP. The MPC CO_2 case presents the highest COP of the MPC cases (at a similar level than the reference), and reduces both the thermal and electrical energy, similarly to what was observed in heating mode.

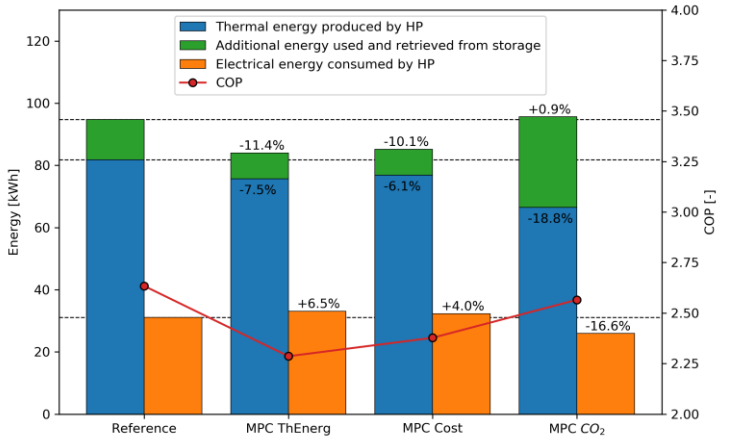

Figure 22. Energy analysis of the cooling cases.

3.2.3. Cost and emissions

The costs and emissions savings are summarized in Table 6. MPC ThEnerg provokes poor results both in economical and environmental terms: it increases both the costs (+12.9%) and the CO_2 emissions (+5.7%). Even though the heat pump thermal energy is not the lowest for that configuration, the total energy used for conditioning the building (including energy retrieved from the storage ΔE) still achieves the lowest value, with 11.4% saved compared to the reference. This result is coherent with the observations made in heating mode.

MPC Cost achieves the highest cost reduction, of -13% in that case, and it corresponds to the expectations since this is the actual objective function of that MPC. Similarly, MPC CO_2 achieves -19.1% reduction in the emissions and thus also achieves its objective. It should be noted that the calculated savings are greater when considering the marginal emissions rather than the average emissions: the latter calculation would result in only -16.8% emissions savings. In the present work, both MPC Cost and MPC CO_2 have shown considerable potential, and they can be equally used depending on which objective one aims towards.

Table 6. Savings of the cooling MPC cases in terms of cost and CO_2 marginal emissions.

MPC objective case		MPC ThEnerg	MPC Cost	MPC CO_2
Cost variation compared to the reference case	**[€]**	+0.36	-0.36	-0.31
	[%]	+12.9%	-13.0%	-10.97%
Thermal energy J_{en} produced by the HP compared to the reference case	**[kWh]**	-6.16	-5.03	-15.35
	[%]	-7.5%	-6.1%	-18.8%
Energy difference between initial and final state ΔE	**[kWh]**	8.3	8.4	29.1
Total energy $(J_{en} + \Delta E)$ variation compared to the reference case	**[kWh]**	-10.8	-9.5	0.8
	[%]	-11.4%	-10.1%	0.9%
Electricity use variation compared to the reference case	**[kWh]**	+2.03	+1.24	-5.15
	[%]	+6.5%	+4.0%	-16.6%
Average CO_2 emissions variation compared to the reference case	**[kgCO_2]**	+0.40	+0.39	-1.22
	[%]	+5.5%	+5.4%	-16.8%
Marginal CO_2 emissions variation compared to the reference case	**[kgCO_2]**	+0.42	+0.37	-1.39
	[%]	+5.7%	+5.0%	-19.1%

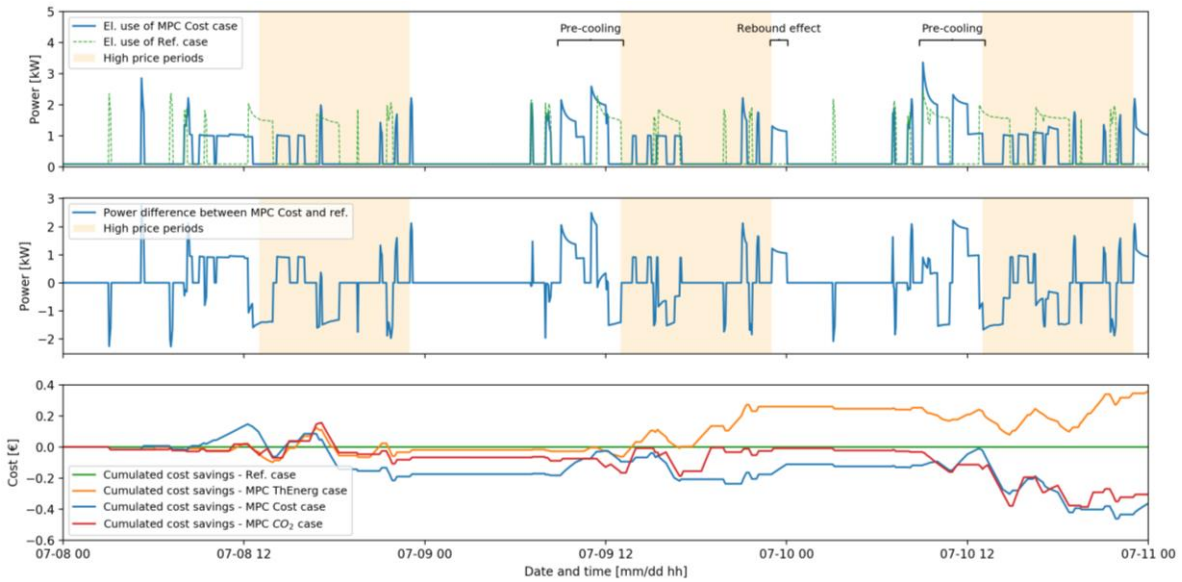

Figure 23. Electricity use of the heat pump in the reference and the MPC Cost cases (top graph), resulting difference (middle graph) and cumulated cost savings of the four studied cases (bottom graph).

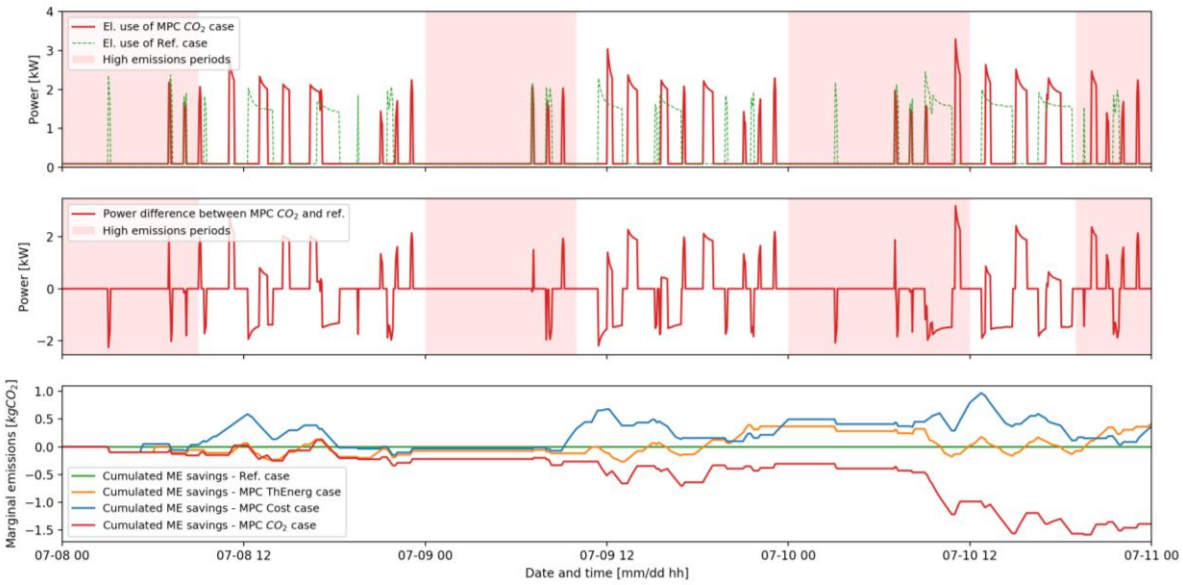

Figure 24. Electricity use of the heat pump in the MPC CO_2 and reference cases (top graph), resulting difference (middle graph) and cumulated marginal emissions savings of the four cases (bottom graph).

Analyzing detailed plots of the costs and emissions outputs helps to understand and endorse the findings of Table 6. For the cost analysis, Figure 23 shows the satisfactory performance of MPC Cost in cooling mode: similarly than in heating mode, the effects of pre-cooling and rebound effect are observed, as a result of the predictive behavior of the controller. During the last day, where the outdoor temperature and solar heat gains are the highest, the cooling load is higher and therefore cannot be shifted entirely to the low price period, some cooling still needs to be provided during the high price period. For the emissions analysis in Figure 24, the load shifting is less evident, but still occurs. MPC CO_2 is the only configuration that manages to reduce the CO_2 emissions, logically achieving its declared objective and saving -1.39 $kgCO_2$ compared to the reference case, hence a reduction of -19.1%.

3.2.4. Comfort

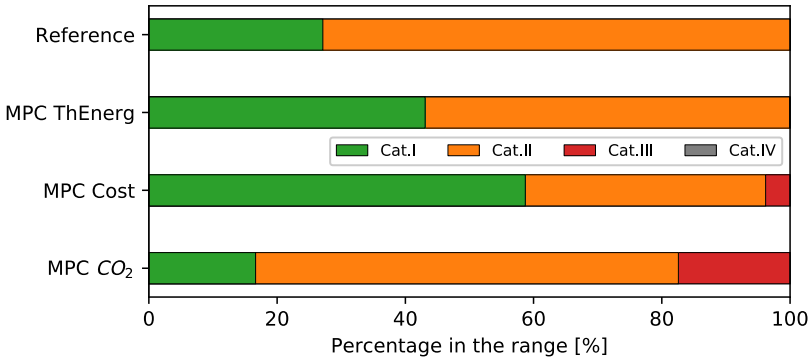

Figure 25. Comfort analysis of the cooling cases.

The comfort analysis for cooling is presented in Figure 25. The comfort categories are adapted for the summer season (Cat.I for instance corresponds to an operative temperature below 25.5°C), still from the European standard EN 15251. It appears that some MPC configurations improve the comfort conditions: in the case of MPC ThEnerg, this improvement obviously has a cost in terms of energy and lack of flexibility. In the case of MPC Cost, comfort is also improved (+31.6% of the time in Cat.I), simultaneously with the previously analyzed indicators: such results highlight the joint benefits that can be attained with predictive controllers. In the case of MPC CO_2, the comfort is slightly degraded due to the low value assigned to α_ε, the weighting coefficient associated with the

comfort objective. As a result, few excursions happen in Cat.III (+17.4%), suggesting that larger fluctuations occur in the indoor environment. However, in all configurations the temperature always stays within the range of Category III, which is considered as the acceptable threshold (operative temperature below 27°C).

4. Discussions on MPC for heat pump control and energy flexibility

4.1. Sensitivity of MPC

The development steps of the MPC controller have been recounted in the present article. Undergoing this process enabled to highlight the large development efforts still needed to build such controllers. For instance, the weighting coefficients required fine tuning for every MPC configurations, and the MPC outcome was greatly influenced by the choice of these parameters. In particular, the value of the coefficient α_ε, associated with the objective J_ε determines whether the controller will rather emphasize comfort or the flexibility objective; it should thus be chosen with specific care. For example in the MPC Cost configuration in cooling mode, $\alpha_\varepsilon = 0.15$ was still a high value since comfort was significantly increased; decreasing it further could have led to even higher savings and comfort conditions closer to the reference case. Considering hard constraints rather than soft ones (hence eliminating the discomfort term J_ε in the objective function) could solve this sensitivity issue, however the J_ε objective considerably improves the robustness of the controller [44] and therefore it remains interesting to keep it.

Adjustments were also needed between the heating and cooling configurations. For example, the weighting coefficients and the RC model parameters have significantly different values for MPC Cost in the two seasons. This could be due to the fact that the electricity price level changes seasonally (the average price is 22% lower in the cooling case than in the heating case), and thus the Pareto analysis compensates for this difference by decreasing accordingly the α_ε coefficient. A more meticulous sensitivity analysis could be conducted on these weighting parameters as a further research topic, for instance trying to obtain coefficients independent from the utilized penalty signal. This could be done by dynamically adapting the coefficients to the level of the input signal, or a prior normalization of the input signal realized in a more dynamic way than the present study (i.e. not considering a fixed maximum cost E_{max}).

4.2. MPC as a tool to activate the energy flexibility of buildings

Despite the identified barriers previously discussed, the proposed MPC framework has shown a good performance for activating the energy flexibility of residential buildings in the Mediterranean area. Operating a building flexibly is a subtle compromise between different aspects that are all related and sometimes contradictory. The strength of MPC is that such control is capable to quantify and balance different objectives. Furthermore, it can sometimes lead to improving several objectives at a time: for instance, the MPC Cost configuration enables simultaneously to realize some load shifting towards low-price periods, to reduce the electricity bill of the users, while maintaining comfortable conditions indoors. These findings are of utmost importance since the deployment of flexibility at a large scale will require the acceptance of all parties involved: the occupants of the buildings (interested in their comfort and energy bills), the grid stakeholders (interested in load shifting and the moments when electricity is consumed) and the society as a whole (which should be concerned about the reduction of the CO_2 emissions and climate change).

The penalty signals play an important role in the activation of building energy flexibility. In the present work, two different signals have been used: the time-varying electricity price and the marginal CO_2 intensity of the grid. From the analyzed cases, it appears that they often display opposite behavior: the high penalty occurs in the afternoons for the price (the grid operators want to incentivize peak shaving in this way), while it corresponds to the low penalty for CO_2 (due to the high share of solar and renewable energy at this moment). The results also show that the patterns of these signals greatly affect the outcome of the MPC controller: the price signal presents large day-night variations, and thus already provides a pre-defined pattern for the electricity use, which

facilitates the consequent optimization of the MPC. On the other hand, the CO_2 signal presents smaller variations, and therefore gives little prior information to the MPC as to which periods are more interesting for operating the systems. The marginal emissions signal was chosen precisely because it varies more than the average emissions signal, but it appeared that this was not sufficient in some cases. Both normalized signals can be seen in Figure 26 for comparison.

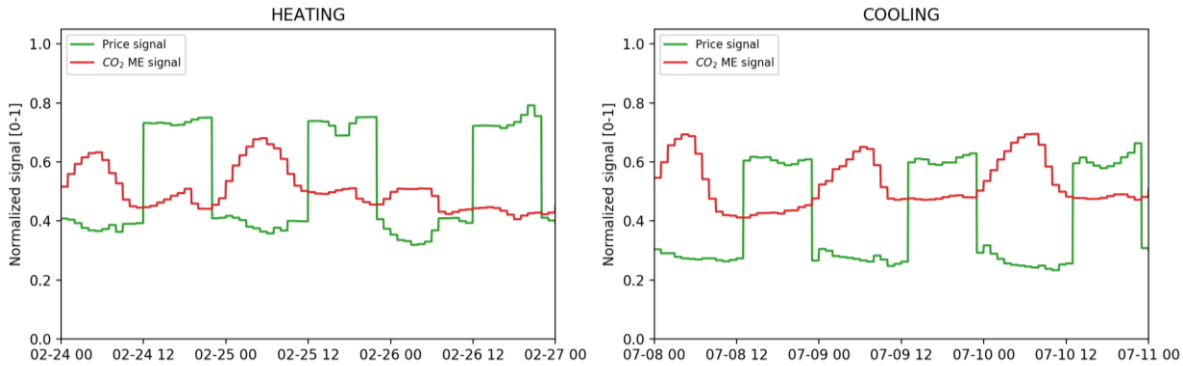

Figure 26. Normalized signals in heating and cooling modes.

Conclusions

From development to application, the present study has covered many aspects of using Model Predictive Control for heat pump control and enhancing the energy flexibility of building thermal loads. Several steps were followed for creating the MPC controller: identification of simplified linear models of the building envelope and of the heat pump performance, definition of different objective functions, software implementation and tuning of the algorithm parameters. This process enabled to highlight the specificities of a controller used for both heating and cooling, and the still consequent development costs of such controller.

A co-simulation framework was then created between TRNSYS and MATLAB to test the created MPC controller. This framework can be reused to test many different aspects of MPC and energy flexibility, and to perform sensitivity analysis on the numerous parameters present in the MPC algorithm and models. In the present case, the MPC controller with three different objective functions (minimization of the thermal energy, of the electricity costs or the CO_2 marginal emissions) was tested on a Spanish residential building in heating and cooling seasons. Among these 3 configurations, MPC Cost performed better in comparison to a traditional thermostatic control: it enabled notably to shift the loads towards low-price periods (FF_{cost} was increased from 0.19 to 0.44 in heating and from -0.20 to 0.27 in cooling), resulting in monetary savings in the range of 13 to 28%. The electricity used by the heat pump controlled by the MPC Cost was also reduced, due to an operation at lower supply temperature, which resulted in a higher efficiency, mostly in heating mode. The MPC controller achieved these positive results without affecting the thermal comfort of the occupants, and therefore constitutes a very promising control technique for enhancing the energy flexibility of buildings. The MPC CO_2 configuration also performed well, although its load-shifting behavior was less evident: it achieved marginal emissions savings in the range of 19 to 29%. On the other hand, MPC ThEnerg did not present the lowest amount of thermal energy produced by the heat pump, even though this was its minimization objective. However, when considering the total thermal energy used to condition the building (hence including also the energy which had been previously stored in the building mass and the water tank, and retrieved during the studied cases), MPC ThEnerg did actually present the highest savings, in the range of 10 to 11%. This reveals that MPC ThEnerg retrieved less energy from the storage than the other MPC cases, leading to a better thermal energy management on the long term. The complexity of the MPC controller and its sensitivity to tuned parameters have additionally been discussed: the good results obtained with the MPC controllers required several adjustments and extensive expertise, which makes a broader implementation still delicate.

943 Given the potentially important benefits brought by MPC controllers and demonstrated in the
944 present work, it is hoped that the computation barriers will become less limiting with the ever
945 increasing calculation capacities. A consequent amount of research has already been dedicated to
946 MPC for building climate control, therefore the further efforts should focus in applying these
947 strategies to real heat pump systems. In this way, potential obstacles in the implementation can be
948 identified, and the performance can be verified against more realistic conditions. In particular, the
949 dynamic effects of the heat pump were neglected in the present work (i.e. we considered that the heat
950 pump reaches the desired set-point always). The discrepancy between the sent commands and the
951 actual operation of the heat pump (delayed response, ramping) will thus be the object of further work
952 based on laboratory experiments.

953 **Nomenclature**

Variables

C	Thermal capacity
e	Vector of external inputs (disturbances)
E	Cost (price or emissions)
f	Frequency
FF	Flexibility factor
gA	Aperture area
I_H	Solar irradiation
J	Objective
m	Flow rate
M	Coefficient of heat conversion
N	Prediction horizon
P	Electrical power
Q	Thermal power (negative for cooling)
R	Thermal resistance
T	Temperature
u	Vector of controlled variables
x	Vector of states
y	Vector of output variables
α	Weighting coefficient
δ	Binary variable (on/off switching)
ΔT	$T_{sup} - T_{ret}$ Water temperature difference
ε	Slack variable (comfort violations)

Indices

S	Space heating or cooling
SH	Space Heating
SC	Space Cooling
TES	Thermal Energy Storage (DHW tank)
DHW	Domestic Hot Water extractions
el	Electricity
sup	Supply
ret	Return
amb	Ambient
occ	Occupants
w	Water
eff	Effective
eq	Equivalent
obj	Objective function: "en", "cost" or "CO2"
en	Objective: minimization of thermal energy
cost	Objective: minimization of the costs
CO2	Objective: minimization of the CO_2 emissions
det	Detailed (heat pump model)
simpl	Simplified (heat pump model)
tot	For both space heating/cooling and DHW
int	Relative to the internal zone state
w	Relative to the wall state
ε	Relative to the comfort objective
Δu	Relative to the smoothing objective
p	Penalty signal (price or emissions)
lp	Low penalty
hp	High penalty
e	Relative to the exogenous inputs
u	Relative to the controllable inputs

Abbreviations

COP	Coefficient of Performance
DHW	Domestic Hot Water
EER	Energy Efficiency Ratio
FCU	Fan-Coil Units
(VS)HP	(Variable Speed) Heat Pump
HVAC	Heating, Ventilation & Air Conditioning
KPI	Key Performance Indicator
LP	Linear Programming
MEF	Marginal Emissions Factor
MILP	Mixed Integer Linear Programming
MPC	Model Predictive Control
OCP	Optimal Control Problem
PLR	Part-Load Ratio
PRBS	Pseudo Random Binary Signal
RES	Renewable Energy Sources
(N)RMSE	(Normalized) Root Mean Square Error

954

Conflicts of Interest: The authors declare no conflict of interest.

References

[1] Intergovernmental Panel on Climate Change (IPCC), "Special Report on Global Warming of 1.5°C," Incheon, Republic of Korea, 2018.

[2] P. D. Lund, J. Lindgren, J. Mikkola, and J. Salpakari, "Review of energy system flexibility measures to enable high levels of variable renewable electricity," *Renewable and Sustainable Energy Reviews*, vol. 45. Elsevier, pp. 785–807, 2015.

[3] C. Mitchell, "Momentum is increasing towards a flexible electricity system based on renewables," *Nat. Energy*, vol. 1, no. 2, p. 15030, 2016.

[4] S. Ø. Jensen, A. Marszal-Pomianowska, R. Lollini, W. Pasut, A. Knotzer, P. Engelmann, A. Stafford, and G. Reynders, "IEA EBC Annex 67 Energy Flexible Buildings," *Energy Build.*, vol. 155, pp. 25–34, Aug. 2017.

[5] Y. Chen, P. Xu, J. Gu, F. Schmidt, and W. Li, "Measures to improve energy demand flexibility in buildings for demand response (DR): A review," *Energy and Buildings*, vol. 177. Elsevier B.V., pp. 125–139, 2018.

[6] A. Arteconi, N. J. Hewitt, and F. Polonara, "State of the art of thermal storage for demand-side management," *Appl. Energy*, vol. 93, pp. 371–389, 2012.

[7] D. Fischer and H. Madani, "On heat pumps in smart grids: A review," *Renew. Sustain. Energy Rev.*, vol. 70, no. October 2016, pp. 342–357, 2017.

[8] T. Q. Péan, J. Salom, and R. Costa-Castelló, "Review of control strategies for improving the energy flexibility provided by heat pump systems in buildings," *J. Process Control*, vol. 74C, no. Special Issue on Efficient Energy Management, pp. 35–49, Apr. 2019.

[9] G. Bianchini, M. Casini, D. Pepe, A. Vicino, and G. G. Zanvettor, "An Integrated MPC Approach for Demand-Response Heating and Energy Storage Operation in Smart Buildings," *IEEE Conf. Decis. Control 2017*, no. Cdc, pp. 3865–3870, 2017.

[10] R. E. Hedegaard, T. H. Pedersen, M. D. Knudsen, and S. Petersen, "Towards practical model predictive control of residential space heating: Eliminating the need for weather measurements," *Energy Build.*, vol. 170, pp. 206–216, 2018.

[11] B. Manrique Delgado, S. Cao, A. Hasan, and K. Sirén, "Multiobjective optimization for lifecycle cost, carbon dioxide emissions and exergy of residential heat and electricity prosumers," *Energy Convers. Manag.*, vol. 154, no. April, pp. 455–469, 2017.

[12] C. Verhelst, F. Logist, J. Van Impe, and L. Helsen, "Study of the optimal control problem formulation for modulating air-to-water heat pumps connected to a residential floor heating system," *Energy Build.*, vol. 45, pp. 43–53, 2012.

[13] G. Lowry, "Day-ahead forecasting of grid carbon intensity in support of heating, ventilation and air-conditioning plant demand response decision-making to reduce carbon emissions," *Build. Serv. Eng. Res. Technol.*, vol. 39, no. 6, pp. 749–760, 2018.

[14] P. J. C. Vogler-Finck, R. Wisniewski, and P. Popovski, "Reducing the carbon footprint of house heating through model predictive control – A simulation study in Danish conditions," *Sustain. Cities Soc.*, vol. 42, no. January, pp. 558–573, 2018.

[15] T. Q. Péan, J. Salom, and J. Ortiz, "Environmental and Economic Impact of Demand Response Strategies for Energy Flexible Buildings," in *Building Simulation and Optimization BSO 2018, 11-12th September 2018, Cambridge (UK)*, 2018.

[16] S. Prívara, J. Široký, L. Ferkl, and J. Cigler, "Model predictive control of a building heating system: The first experience," *Energy Build.*, vol. 43, no. 2–3, pp. 564–572, 2011.

[17] H. Thieblemont, F. Haghighat, R. Ooka, and A. Moreau, "Predictive control strategies based on weather forecast in buildings with energy storage system: A review of the state-of-the art," *Energy Build.*, vol. 153, pp. 485–500, 2017.

[18] N. Alibabaei, A. S. Fung, and K. Raahemifar, "Development of Matlab-TRNSYS co-simulator for applying predictive strategy planning models on residential house HVAC system," *Energy Build.*, vol. 128, pp. 81–98, 2016.

[19] J. Lofberg, "YALMIP : a toolbox for modeling and optimization in MATLAB," *2004 IEEE Int. Conf. Robot. Autom. (IEEE Cat. No.04CH37508)*, pp. 284–289, 2004.

[20] Gurobi Optimization, "Gurobi." http://www.gurobi.com, 2018.

[21] J. Ortiz, F. Guarino, J. Salom, C. Corchero, and M. Cellura, "Stochastic model for electrical loads in Mediterranean residential buildings: Validation and applications," *Energy Build.*, vol. 80, pp. 23–36, 2014.

[22] P. Taddeo, J. Ortiz, J. Salom, E. Lucas Segarra, V. Gutiérrez González, G. Ramos Ruiz, and C. Fernández Bandera, "Comparison of experimental methodologies to estimate the air infiltration rate in a residential case study for calibration purposes," in *39th AIVC 2018 - Smart Ventilation for Buildings - 18-19th September 2018*, 2018.

[23] C. Ghiaus and I. Hazyuk, "Calculation of optimal thermal load of intermittently heated buildings," *Energy Build.*, vol. 42, no. 8, pp. 1248–1258, 2010.

[24] R. De Coninck and L. Helsen, "Practical implementation and evaluation of model predictive control for an office building in Brussels," *Energy Build.*, vol. 111, pp. 290–298, 2016.

[25] H. Johra and P. Heiselberg, "Influence of internal thermal mass on the indoor thermal dynamics and integration of phase change materials in furniture for building energy storage: A review," *Renew. Sustain. Energy Rev.*, vol. 69, no.

May 2016, pp. 19–32, 2017.
[26] G. Reynders, J. Diriken, and D. Saelens, "Quality of grey-box models and identified parameters as function of the accuracy of input and observation signals," *Energy Build.*, vol. 82, 2014.
[27] H. Viot, A. Sempey, L. Mora, J. C. Batsale, and J. Malvestio, "Model predictive control of a thermally activated building system to improve energy management of an experimental building: Part I—Modeling and measurements," *Energy Build.*, vol. 172, pp. 94–103, 2018.
[28] CEN, "EN 12976-2 - Thermal solar systems and components - Factory made systems - Part 2: Test methods." Brussels, Belgium, 2017.
[29] P. Bacher and H. Madsen, "Identifying suitable models for the heat dynamics of buildings," *Energy Build.*, vol. 43, no. 7, pp. 1511–1522, 2011.
[30] H. Madsen, P. Bacher, G. Bauwens, A.-H. Deconinck, G. Reynders, S. Roels, E. Himpe, and G. Lethé, "Thermal Performance Characterization using Time Series Data - IEA EBC Annex 58 Guidelines," 2015.
[31] L. Ljung, *MATLAB System Identification Toolbox - Getting Started Guide R2016a*. Mathworks, 2016.
[32] K. A. Antonopoulos and E. Koronaki, "Apparent and effective thermal capacitance of buildings," *Energy*, vol. 23, no. 3, pp. 183–192, Mar. 1998.
[33] Y. J. Kim, E. Fuentes, and L. K. Norford, "Experimental Study of Grid Frequency Regulation Ancillary Service of a Variable Speed Heat Pump," *IEEE Trans. Power Syst.*, vol. 31, no. 4, pp. 3090–3099, 2016.
[34] G. St-Onge, M. Kummert, and M. Kegel, "Variable capacity mini-split air source heat pump model for TRNSYS," in *eSim 2018, the 10th Conference of IBPSA-Canada*, 2018.
[35] CEN, "EN 14511-2: Air conditioners, liquid chilling packages and heat pumps with electrically driven compressors for space heating and cooling - Part 2: Test conditions." Brussels, Belgium, 2012.
[36] J. Maciejowski, *Predictive control with constraints*. 2002.
[37] Red Electrica de España, "ESIOS – Sistema de información del operador del sistema.," 2018. [Online]. Available: https://www.esios.ree.es/en (accessed 07/03/2018). [Accessed: 04-Apr-2017].
[38] J. Le Dréau and P. Heiselberg, "Energy flexibility of residential buildings using short term heat storage in the thermal mass," *Energy*, vol. 111, no. 1, pp. 1–5, 2016.
[39] T. Q. Péan, J. Salom, and J. Ortiz, "Potential and optimization of a price-based control strategy for improving energy flexibility in Mediterranean buildings," *CISBAT 2017 Int. Conf. – Futur. Build. Dist. – Energy Effic. from Nano to Urban Scale, CISBAT 2017 6-8 Sept. 2017, Lausanne, Switz.*, vol. 122, pp. 463–468, 2017.
[40] European Commission, *2013/114/EU Commission Decision of 1 March 2013 establishing the guidelines for Member States on calculating renewable energy from heat pumps from different heat pump technologies pursuant to Article 5 of Directive 2009/28/EC of the European Parliament an*, no. March. 2013, pp. 27–35.
[41] J. Pospíšil, M. Špiláček, and L. Kudela, "Potential of predictive control for improvement of seasonal coefficient of performance of air source heat pump in Central European climate zone," *Energy*, vol. 154, pp. 415–423, 2018.
[42] P. Morales-Valdés, A. Flores-Tlacuahuac, and V. M. Zavala, "Analyzing the effects of comfort relaxation on energy demand flexibility of buildings: A multiobjective optimization approach," *Energy Build.*, vol. 85, pp. 416–426, 2014.
[43] CEN, "EN 15251: Indoor environmental input parameters for design and assessment of energy performance of buildings addressing indoor quality, thermal environment, lighting and acoustic." European Committee for Standardization, Brussels, Belgium, 2007.
[44] G. Masy, E. Georges, C. Verhelst, and V. Lemort, "Smart grid energy flexible buildings through the use of heat pumps and building thermal mass as energy storage in the Belgian context," *Sci. Technol. Built Environ.*, vol. 4731, no. August, pp. 800–811, 2015.